Patterned piezo-, pyro-, and ferroelectricity of poled polymer electrets

Cite as: J. Appl. Phys. **108**, 011101 (2010); https://doi.org/10.1063/1.3457141
Submitted: 29 January 2010 • Accepted: 26 May 2010 • Published Online: 12 July 2010

Xunlin Qiu

APPLIED PHYSICS REVIEWS—FOCUSED REVIEW

Patterned piezo-, pyro-, and ferroelectricity of poled polymer electrets

Xunlin Qiu[a)]
Department of Physics and Astronomy, Applied Condensed-Matter Physics, University of Potsdam, Karl-Liebknecht-Strasse 24-25, 14476 Potsdam-Golm, Germany

(Received 29 January 2010; accepted 26 May 2010; published online 12 July 2010)

Polymers with strong piezo-, pyro-, and ferroelectricity are attractive for a wide range of applications. In particular, semicrystalline ferroelectric polymers are suitable for a large variety of piezo- and pyroelectric transducers or sensors, while amorphous polymers containing chromophore molecules are particularly interesting for photonic devices. Recently, a new class of polymer materials has been added to this family: internally charged cellular space-charge polymer electrets (so-called "ferroelectrets"), whose piezoelectricity can be orders of magnitude higher than that of conventional ferroelectric polymers. Suitable patterning of these materials leads to improved or unusual macroscopic piezo-, pyro-, and ferroelectric or nonlinear optical properties that may be particularly useful for advanced transducer or waveguide applications. In the present paper, the piezo-, pyro-, and ferroelectricity of poled polymers is briefly introduced, an overview on the preparation of polymer electrets with patterned piezo-, pyro-, and ferroelectricity is provided and a survey of selected applications is presented. © *2010 American Institute of Physics*. [doi:10.1063/1.3457141]

TABLE OF CONTENTS

I. INTRODUCTION

Polymers are very widely used in our daily life and in practically all areas of technology. Typical features of polymer materials are flexibility, softness, light weight, relatively low acoustic impedance, low thermal conductivity, etc. Polymer electrets, dielectric materials with a quasipermanent excess charge or dipolar polarization, including semicrystalline ferroelectric polymers and amorphous chromophore-doped nonlinear optical (NLO) polymers have been discussed in this journal for sensors and photonics applications in 1996.[1] For details of the history and the state of the art in 1996 the reader is referred to this review paper and the literature cited therein. Today, semicrystalline poly(vinylidene fluoride) (PVDF) and its copolymers with trifluoroethylene [P(VDF-TrFE)] belong to the electroactive polymers that have been most extensively investigated and applied in numerous practical devices. A number of further ferroelectric polymers have also been discovered and explored, including aromatic and aliphatic polyurea, copolymers of vinylidene cyanide (VDCN), odd-numbered polyamides, poly-L-lactic acid (PLLA), and many bipolymers and synthetic polypeptides, etc.[2–7]

Figure 1 shows the molecular compositions of some ferroelectric polymers. A remarkable and promising development is the emergence of relaxor ferroelectric polymers that can be obtained by introducing additional defects into ferroelectric P(VDF-TrFE) polymer either by means of high-energy irradiation or via copolymerization with a bulky monomer such as chlorofluoroethylene or chlorotrifluoroethylene in order to form a terpolymer. This recent class of soft polymers exhibits extremely large electrostriction response and many features typically also found in relaxor inorganic ferroelectrics.[8] For amorphous chromophore-doped NLO polymers, significant progress has been achieved both in fundamental research and in the development of applications.

[a)]Electronic mail: xunlin@canopus.physik.uni-potsdam.de

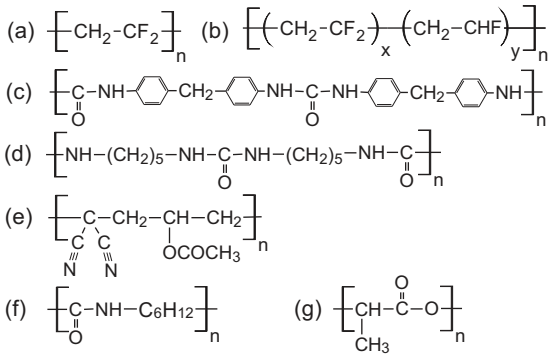

FIG. 1. Molecular compositions of piezoelectric polymers. (a) PVDF, (b) P(VDF-TrFE), (c) aliphatic polyurea, (d) aliphatic polyurea 5, (e) poly(vinylidene-cyanide-co-vinylacetate), (f) Polyamide 7 (PA-7), and (g) PLLA.

For example, the photoinduced motion of chromophores was comprehensively studied both theoretically and experimentally.[9–12] During the last two decades, numerous chromophores have been synthesized, characterized, and incorporated into a polymer matrices by means of physical doping or chemical attachment, in some cases with additional crosslinking.[13–19] Representative chemical compositions of polymers often used as host materials for NLO chromophores are shown in Fig. 2. Additionally, a variety of dendrimers have been prepared in recent years. They are particularly interesting as host materials because of their special well-controlled three-dimensional (3D) architectures.[20,21]

Recently, the family of piezo-, pyro-, and ferroelectric polymers has received a new member called "ferroelectrets" (i.e., internally charged polymer foams). Already during the 1970s, piezo- and pyroelectric properties of noncentrosymmetric electrically charged nonpolar polymers were theoretically predicted and also experimentally studied to some extent.[22,23] However, the research interest faded because of the rather weak piezo- and pyroelectricity obtained at that time. The situation changed substantially over the past one and half decades and a considerable number of cellular and voided electret polymers with strong piezoelectricity were identified and developed. This exciting development[24–27] significantly enlarges the range of piezo- and pyroelectric materials. During electrical poling of cellular or void-containing

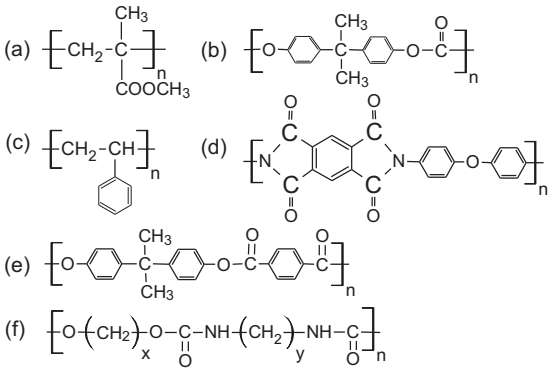

FIG. 2. Molecular compositions of polymers that are often used as matrix materials for chromophores. (a) PMMA, (b) polycarbonate, (c) PS, (d) polyimide, (e) poly (4,4′-isopropylidenediphenylene terephthalate) copolymer (U-100), (f) Polyurethane.

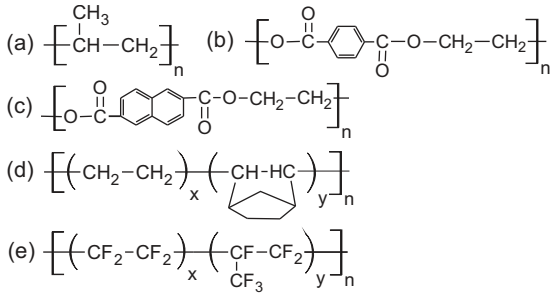

FIG. 3. Chemical compositions of several polymers suitable for ferroelectret preparation. (a) PP, (b) poly(ethylene terephthalate), (c) poly(ethylene naphthalene-2,6-dicarboxylate), (d) cyclo-olefin copolymer, (e) FEP copolymer.

polymer structures, charges of opposite polarity are generated in a dielectric barrier discharge (DBD) and trapped at the internal surfaces of the gas-filled voids.[28–30] The charged voids can be considered as macroscopic dipoles, which—in combination with the macroscopically nonuniform elastic properties of the material—induce the desired piezo- and pyroelectricity. The poled materials are called ferroelectrets because their macroscopic polarization and other related properties are phenomenologically similar to the behavior observed on typical ferroelectrics, while the internal charge trapping is the same as in other space-charge electrets.[31] Figure 3 shows the chemical compositions of several polymers that have been successfully employed to develop ferroelectrets.[32–37] Depending on the structure of the material and the charging conditions, ferroelectrets often show piezoelectric d_{33} coefficients of hundreds of pC/N, more than an order of magnitude greater than those found in conventional ferroelectric polymers and comparable to the values found in advanced ferroelectric ceramics. Consequently, the new ferroelectrets have attracted considerable interest in research and industry.

The three types of relevant polymer electrets are schematically summarized in Fig. 4. For details on the recent development in this area, the interested reader may consult the respective reviews, such as Refs. 2–7 for ferroelectric polymers, Refs. 9–21 for NLO polymers, and Refs. 24–27 for polymer ferroelectrets, as well as the literature cited therein. Research on piezoelectric composites is also very active. In view of the relatively small piezo- and pyroelectric coefficients of ferroelectric polymers, polymer-ceramic composites—usually ceramic particles embedded in a suitable polymer matrix—are prepared in order to combine the respective advantages of polymers (as above-mentioned) and of ceramics: strong piezo- and pyroelectricity, low dielectric and mechanical loss, a large range of possible dielectric permittivities, etc. Experimental and theoretical studies reveal that the composites possess hybrid properties of the constituents.[38–41] The same basic concept was recently adopted by Ganesan *et al.*[42,43] for a different type of composite. Liquid-crystal (LC) droplets are dispersed in ferroelectric P(VDF-TrFE). After poling of the P(VDF-TrFE) matrix, the local electric field across the LC-filled cavities acts on the LC molecules as a bias field. Due to the piezoelectric effect, the internal electric field of the film changes upon

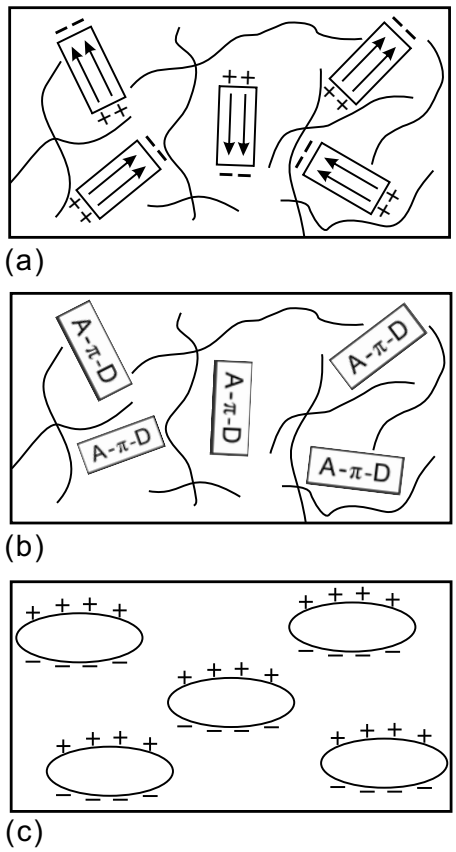

FIG. 4. Schematic view of piezo-, pyro-, and ferroelectric polymer electrets. (a) In semicrystalline ferroelectric polymers, ferroelectric crystallites are dispersed in the amorphous matrix. Space charges trapped at the interfaces between crystallites and amorphous matrix compensate and stabilize the ferroelectric polarization (Ref. 1). (b) Amorphous polymers for photonics applications contain chromophore molecules with large hyperpolarizabilities and large dipole moments (Ref. 1). (c) A new member of the family of piezo-, pyro-, and ferroelectric polymer electrets: internally charged nonpolar cellular polymers with very high piezoelectricity. Charges of opposite sign are deposited on the internal top and bottom surfaces of the voids so that the charged voids can be considered as macroscopic dipoles.

variations in the external mechanical stress, leading to a change in the optical transmission of the composite film. Such a piezo-optical composite may be very attractive for applications e.g., in sensing and visualization but it is also interesting from a fundamental point of view, since the interaction between liquid crystal and ferroelectric polymer can be studied in various ways.

Materials with patterned dipole orientation and thus also patterned piezo-, pyro-, and ferroelectricity are useful for a variety of applications such as sensor arrays with reduced cross talk between individual elements, piezoelectric gratings for direction-sensitive acoustic-wave detection or emission, pyroelectric sensor arrays with complex shapes, etc. For modal-dispersion phase matching within NLO polymer waveguides, steplike dipole orientation profiles across the polymer thickness are usually required.[44] In this paper, we discuss the patterning of piezo-, pyro-, and ferroelectric polymer electrets along their thickness or lateral directions on micro- and macroscopic scales. Obviously, microprocessing and nanofabrication techniques that are widely employed in the manufacture of micro- and optoelectronic devices can also be used for the patterning of functional structures. A comprehensive survey of these sophisticated techniques is not attempted here. For details, the interested reader may refer to pertinent references such as Refs. 45–49 and to the literature quoted therein. Nevertheless, some of the techniques related to polymer electrets have to be briefly introduced.

The present review starts with a thermodynamic definition of piezo-, pyro-, and ferroelectricity and with a description of the modifications that are necessary in order to account for these effects in poled polymers. The piezo- and pyroelectricity, as well as the NLO properties in polar polymers are briefly reviewed. This is followed by a comprehensive discussion about the poling of ferroelectrets and the resulting piezoelectricity. In Sec. III, suitable techniques for patterning piezo-, pyro-, and ferroelectric polymers are reviewed. It is possible to induce desired polarization patterns into initially homogeneous polymer films by means of selective poling and/or depoling techniques. Patterned polarization can also result from patterned sample structures directly formed during sample preparation. In Sec. IV, several representative applications are shown in order to highlight the applications potential of polymers with patterned piezo-, pyro-, and ferroelectricity. It will become evident from the discussion that suitable combinations of different patterning techniques lead to electroactive polymers with complex polarization patterns, allowing for innovative devices. Conclusions about the topics reviewed here will be drawn in Sec. V.

II. PIEZO-, PYRO-, AND FERROELECTRICITY IN POLED POLYMER ELECTRETS

Ferroelectricity is based on spontaneous polarization in the material, the direction of which can be switched or modified by external electric fields. An essential criterion for ferroelectricity is the hysteresis behavior of the electric polarization as a function of the electric field. Materials with ferroelectricity are always piezo- and pyroelectric as well.

Defined in a rigorous way according to thermodynamical principles, the macroscopic piezoelectric d_{mj} coefficient is a tensor component given by the second derivative of the Gibbs free energy G with respect to the electric field vector E and the stress tensor X,[50]

$$d_{mj} = \left[\frac{\partial^2 G(E,X,T)}{\partial E_m \partial X_j} \right]_T, \tag{1}$$

where T is the temperature. Similarly, the pyroelelctric p_m coefficient is defined as

$$p_m = \left[\frac{\partial^2 G(E,X,T)}{\partial E_m \partial T} \right]_X. \tag{2}$$

The second derivatives in Eqs. (1) and (2) can be taken in any order so that

$$d_{mj} = \left(\frac{\partial D_m}{\partial X_j} \right)_{T,E} = \left(\frac{\partial x_j}{\partial E_m} \right)_{X,T} \tag{3}$$

and

$$p_m = \left(\frac{\partial D_m}{\partial T}\right)_E = \left(\frac{\partial S}{\partial E_m}\right)_T, \tag{4}$$

where D, x, and S are the electric displacement, the strain, and the entropy, respectively. The first expression in Eq. (3) denotes the direct piezoelectric (transducer) effect, while the second expression describes the inverse piezoelectric (actuator) effect. Thus, the reciprocity of direct and inverse piezoelectricity immediately follows from the theoretical treatment.

For practical purposes, the piezo- and pyroelectric coefficients in polymers can often be defined by a single expression[51]

$$\xi = \frac{1}{A}\left(\frac{\partial Q}{\partial \Xi}\right), \tag{5}$$

where ξ is either the piezo- or the pyroelectric coefficient, Ξ is the pressure p or the temperature T, and A and Q are the electroded area and the charge on the measuring electrode, respectively. In Eq. (5), only commonly measured quantities are involved.

A. Polar polymers

In a number of reviews on polar polymers with piezo- and pyroelectricity (see for instance, Refs. 1–7), the physical basis, typical experimental results and suggested or implemented applications are extensively discussed.

It is generally accepted that the main contribution to the piezo- and pyroelectricity in polar polymers arises from the dipole-density change as a result of dimensional changes in the sample upon compression (secondary piezoelectricity) or thermal expansion (secondary pyroelectricity). In semicrystalline polymers, dipole libration, reversible changes in crystallinity, and motion of charges necessary for the compensation of the crystallite polarization may also affect the piezo- and pyroelectricity to some extent, while the effect of the affine motion of the dipoles should be taken into account in amorphous polar polymers. Four requirements should be fulfilled for large piezo- and pyroelectricity in polymers:[3] (1) molecular dipoles must be present with a large dipole moment and at a sufficient concentration. (2) The dipoles must be preferentially aligned by a poling procedure and the best results are obtained when saturation is achieved. (3) The dipole alignment, once achieved, must be locked-in, where the best results are obtained in thermodynamically stable states or in frozen states far away from softening temperatures. (4) For piezoelectricity, the material should be easily strained with applied stress, whereas pyroelectricity requires a significant (reversible) temperature dependence of the polarization, often resulting from a relatively large thermal expansion of the relevant phase.

NLO behavior is another important property associated with oriented dipoles in polar polymers. However, it was found that the NLO susceptibility of semicrystalline polar polymer is usually too weak for any practical applications. More recently, a new class of amorphous polymers that contain chromophore molecules with large hyperpolarizabilities and large dipole moments emerged. After the molecular dipoles are preferentially oriented by means of poling, the amorphous NLO polymers show significant second-order NLO effects, and therefore, have numerous applications in photonics and optoelectronics.[19,21]

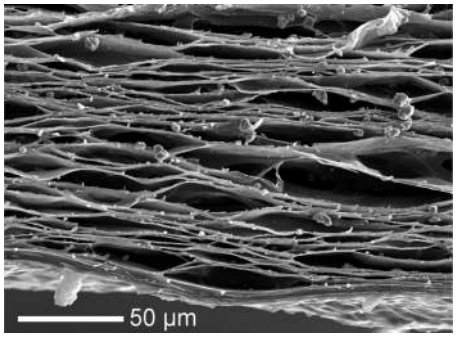

FIG. 5. Scanning electron micrograph of the cross section of a cellular PP foam (Ref. 52).

B. Ferroelectrets

Usually, ferroelectricity is only expected in polar materials. Thus, it came as a big surprise that completely nonpolar polymers with internal space charge of both polarity—the so-called ferroelectrets—behave almost like ferroelectrics! Because of their unusual features, ferroelectrets attract more and more attention both from science and industry. For recent reviews the reader is referred to Refs. 24–27. In this subsection, some new results concerning the poling process in ferroelectrets are discussed. The layer model for the piezoelectricity in ferroelectrets, which consists of alternating polymer and air layers, is also introduced here, since it has not been covered in detail within the above-mentioned review articles.

1. Poling

As seen in the scanning electron microscope (SEM) image of a typical cellular polypropylene (PP) foam in Fig. 5, a large number of voids, with lateral dimensions on the order of 100 μm and vertical dimensions of up to approximately 10 μm, are distributed throughout the bulk of the foamed polymer film.[52] In order to render polymer foams piezoelectric, the voids must be internally charged. The poling process in ferroelectrets is based on DBDs. In DBDs, at least one side of the discharge gap is insulated from the electrodes by a dielectric layer. Based on the investigation of the light emission from the DBDs in ferroelectrets during poling,[28] a schematic model for the poling process has been proposed.[29] Internal breakdown (Paschen breakdown) in the voids is triggered when the electric field in the voids reaches the required threshold value (comparable with the "coercive field" in ferroelectrics). Charges of opposite polarity are separated in the very high electric field inside the DBD and are subsequently trapped on the top and bottom surfaces of the voids, respectively (point A in Fig. 6). The trapped charges induce an internal electric field opposite to the externally applied field and thus extinguish the discharge. As the applied voltage increases further, a second breakdown may occur, and the density of the internally trapped charges strongly increases

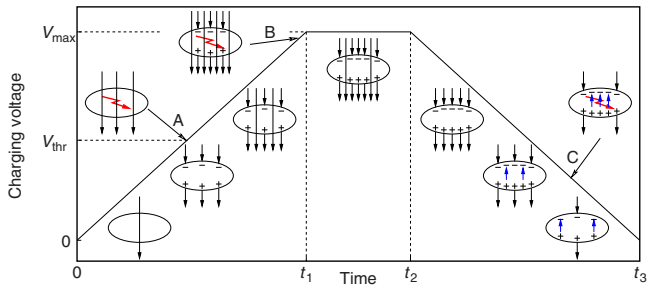

FIG. 6. (Color online) Schematic view of the poling process in a single polymer void. When the poling voltage reaches the threshold value V_{thr}, Paschen breakdown is initiated (a). At higher voltages, a second series of discharges may occur (b). During ramping down the voltage, the reverse electric field from the trapped space charge may lead to back discharges (c) (Ref. 29).

(point B in Fig. 6). When the applied voltage is reduced, the electric field of the trapped charges may overcompensate the applied field and may trigger back discharges (point C in Fig. 6). An *in situ* acoustical monitoring of the polarization build-up in ferroelectrets shows that the back discharges destroy a significant proportion of the effective charge density.[53] In order to optimize the poling efficiency, the geometry (especially the height) of the voids, the type of gas and its pressure inside the voids are critical factors to be considered and to be optimized.[52,54,55]

A direct proof of the internally trapped charges was obtained by means of SEM images.[56] SEM images of obliquely cut cellular PP ferroelectrets provide a direct visualization of negative charges, because the secondary electron-emission yield and the backscatter from negatively charged areas is higher than that from positively charged areas. Overall, the charged voids can be considered as macroscopic dipoles [see, Fig. 4(c)], the direction of which can be reversed by sufficiently high electric fields. Consequently, the resulting electric-displacement versus electric-field curves exhibit hysteresis behavior. It should be noted that DBDs produce a variety of species including energetic and reactive monoatomic as well as molecular diatomic charged particles (i.e., ions), electrons, and neutral species. Therefore, the inner surfaces of the voids in ferroelectrets are exposed to a highly reactive plasma during DBD poling. Both chemical and physical processes occur on the exposed surface areas. Such effects may be used for surface modification, as shown recently in a simple DBD configuration to improve cell adhesion, by means of labeling of fluorophores.[57] It is also found that repeated DBD poling in air leads to the oxidation of the inner surfaces of the voids in cellular PP ferroelectrets and thus deteriorates their chargeability, resulting in significant fatigue of the effective polarization.[58]

2. Piezo- and pyroelectricity

The practical definition of piezo- and pyroelectricity in Eq. (5) holds for ferroelectrets as well. However, the microscopic origin of the piezo- and pyroelectricity in ferroelectrets is significantly different than in polar polymer ferroelectrics. In ferroelectrets, the point symmetry is broken on the macroscopic level with void dimensions on the order of $100\times100\times10$ μm^3, while in polar polymers like PVDF,

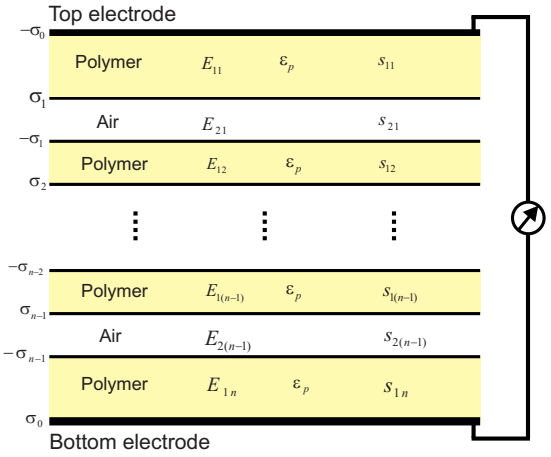

FIG. 7. (Color online) Simplified layer model for ferroelectrets with alternating polymer and air layers (Refs. 59 and 60). Charges of opposite polarity are generated during the DBDs and deposited on the top and bottom air-polymer interfaces, respectively.

the unit cell dimensions are in the order of $0.9\times0.5\times0.3$ nm^3. Thus, the basic dipolar unit in ferroelectrets is 15 orders of magnitude larger than that in ferroelectric polymers. Because of the anisotropy of the lenslike voids and the low symmetry of the charge distribution, high piezoelectric sensitivity is only found in the thickness direction (d_{33} coefficient) and is typically two orders of magnitude larger than the in-plane piezoelectric sensitivity (d_{31} and d_{32} coefficients).

Since the lateral dimensions of the voids are much larger than their vertical dimensions (see, Fig. 5), a simplified model has been proposed to describe the piezoelectricity of ferroelectrets, which consists of consecutive polymer and air layers of thicknesses s_{1i} and s_{2j}, respectively, with $i=1,2,\ldots,n$ and $j=1,2,\ldots,n-1$, where n is the total number of solid layers.[59,60] Figure 7 schematically shows the layer model. The permanent charges on the two sides of each air gap are taken to be equal in magnitude, since it is assumed that they originate from the DBDs in the air gap during poling (which only leads to charge separation but not to the generation of excess charges of one polarity).

The electric fields in the polymer and air layers may be calculated by use of Gauss' and Kirchhoff's laws. For the top and bottom electrodes, Gauss' law can be written as

$$-\varepsilon_0\varepsilon_p E_{11} = -\sigma_0 \tag{6}$$

and

$$\varepsilon_0\varepsilon_p E_{1n} = \sigma_0. \tag{7}$$

For the top and bottom interfaces of the jth air gap,

$$-\varepsilon_0 E_{2j} + \varepsilon_0\varepsilon_p E_{1j} = \sigma_j \tag{8}$$

and

$$-\varepsilon_0\varepsilon_p E_{1(j+1)} + \varepsilon_0 E_{2j} = -\sigma_j. \tag{9}$$

Under short-circuit conditions, Kirchhoff's second law is given by

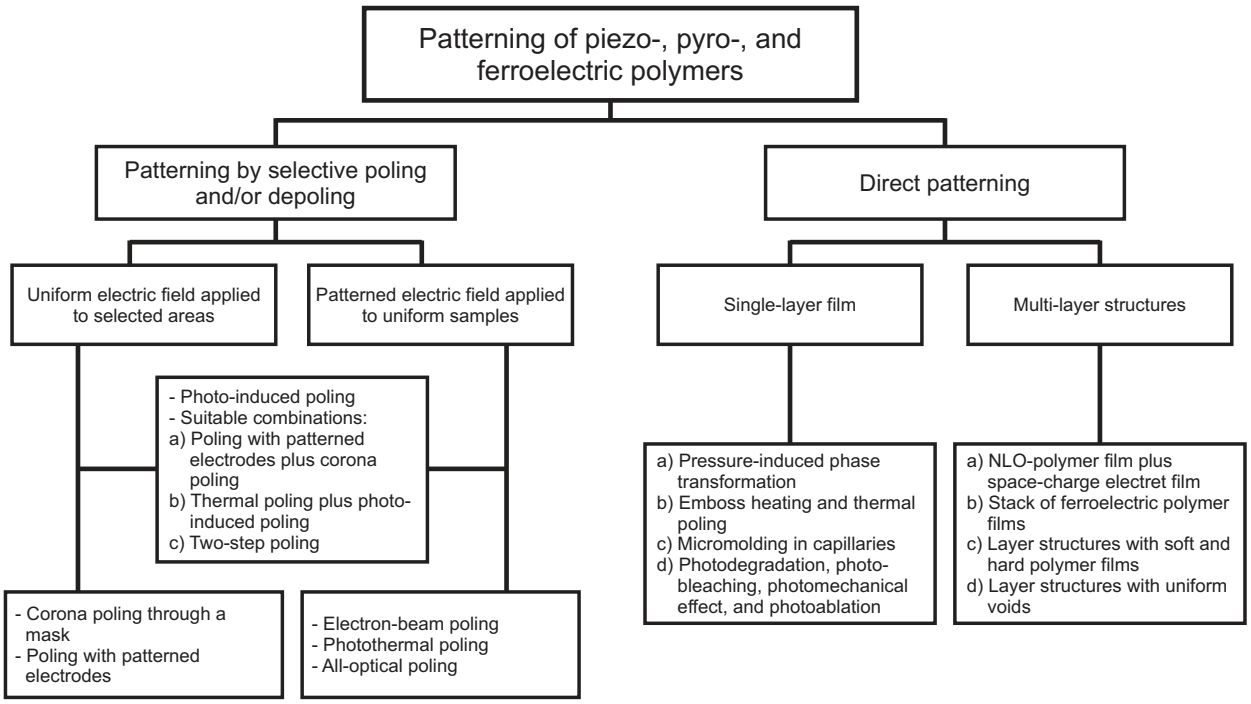

FIG. 8. Schematic illustration of the techniques for patterning piezo-, pyro-, and ferroelectric polymers.

$$\sum_i s_{1i}E_{1i} + \sum_j s_{2j}E_{2j} = 0. \tag{10}$$

Equations (8) and (9) yield

$$E_{11} = E_{12} = \ldots = E_1 \tag{11}$$

and

$$E_{2j} = \varepsilon_p E_1 - \frac{\sigma_j}{\varepsilon_0}. \tag{12}$$

Substituting Eqs. (11) and (12) into Eq. (10), one obtains

$$E_1 = \frac{\Sigma_j s_{2j}\sigma_j}{\varepsilon_0 s_1 + \varepsilon_0 \varepsilon_p s_2} \tag{13}$$

and

$$E_{2i} = \frac{\varepsilon_p \Sigma_j s_{2j}\sigma_j}{\varepsilon_0 s_1 + \varepsilon_0 \varepsilon_p s_2} - \frac{\sigma_i}{\varepsilon_0}, \tag{14}$$

where $s_1 = \Sigma_i s_{1i}$ and $s_2 = \Sigma_j s_{2j}$ are the combined total thicknesses of the polymer and air layers, respectively.

When a pressure p is applied to the electrically charged foam, the thickness changes are primarily due to the compression of the air layers. Therefore, the electrode charge varies according to $\partial\sigma_0/\partial s_2$. If $\partial s_{2j}/\partial s_2 = s_{2j}/s_2$ is assumed, then

$$\frac{\partial\sigma_0}{\partial s_2} = \frac{\varepsilon_p s_1}{(s_1 + \varepsilon_p s_2)^2}\sigma_{\text{eff}}, \tag{15}$$

where $\sigma_{\text{eff}} = \Sigma_j s_{2j}\sigma_j / s_2$ is the effective polarization in the ferroelectret. Together with the stress-strain relation $\Delta s_2/s = p/Y$, where $s = s_1 + s_2$ and Y is Young's modulus of the foam, one obtains the piezoelectric coefficient

$$d_{33} = \frac{\varepsilon_p s}{Y}\frac{s_1\sigma_{\text{eff}}}{(s_1 + \varepsilon_p s_2)^2}. \tag{16}$$

On the other hand, an ac or dc voltage ΔV applied to the layer system generates additional fields e_1 and e_2 in the polymer and air layers, respectively. The field e_2 results in an additional force between the two adjacent polymer layers and hence in a thickness change Δs_{2j} of the air layer in between. By analyzing the sum of the thickness changes Δs_2 and the applied voltage, one obtains the inverse piezoelectric d_{33} coefficient of the ferroelectret[61,62]

$$\frac{\Delta d}{\Delta V} = d_{33}, \tag{17}$$

which confirms the reciprocity of the piezoelectric sensor and actuator effects.

For a comparison of the piezo- and pyroelectricity in ferroelectrets and in ferroelectrics, see, Ref. 26. Due to the high compressibility of the voids, very large piezoelectric d_{33} coefficients of hundreds of pC/N can often be achieved in ferroelectrets. However, the pyroelectric coefficient of ferroelectrets (typically around 0.25 μC/(m^2 K)) is much smaller than that of polar polymers such as PVDF [typically around 27 μC/(m^2 K)], which is an advantage in electromechanical applications, since the respective devices will be relatively insensitive to temperature changes.[63]

III. PATTERNING OF POLED PIEZO-, PYRO-, AND FERROELECTRIC POLYMERS

In this section, the techniques for patterning piezo-, pyro-, and ferroelectric polymers will be discussed. An overview of the proposed patterning techniques is given in Fig. 8. Poling under an electric field is necessary in order to render

piezo-, pyro-, and ferroelectric polymer electrets electroactive. Although poling itself means an additional processing step, it also introduces a degree of freedom in the design of devices. Suitable polarization patterns in the film plane and/or across the film thickness are possible through selective poling as well as depoling techniques. Furthermore, patterned piezo-, pyro-, and ferroelectricity in polymers may directly originate from patterned sample structures introduced by means of suitable sample-preparation procedures.

A. Patterning by selective poling and/or depoling

Poling techniques suitable for breaking the symmetry of polymer electrets have already been reviewed in Ref. 1. In particular, the patterning of piezo-, pyro-, and ferroelectric polymer electrets by means of suitable poling techniques has been discussed in that review. In the following subsections, the possibility of patterning by means of selective poling and/or depoling will be discussed, with a focus on more recent progresses achieved since 1996. A thorough review on the relevant poling techniques themselves will not be given here. Interested readers may refer to the previous review and to the literature cited therein.

1. Corona poling through a mask

Corona discharges have been employed in order to charge the surfaces of electrets since several decades.[64] In addition to established corona-poling procedures for ferroelectric and NLO polymers, corona poling is now also widely used for poling ferroelectrets. In this case, corona poling is often implemented without a grid. The corona ions are deposited onto the surface of the ferroelectret sample and generate a surface potential. Breakdown of the gas inside the voids is triggered when the internal electric field induced by the surface potential reaches the respective threshold. The light emission from the internal breakdown events during corona poling may be recorded with a digital camera.[65] Usually, no thermal treatment is required for triggering the breakdown of the gas inside the voids during corona charging of ferroelectret polymers. This is different from the situation of ferroelectric and NLO polymers, where a simultaneous thermal treatment is usually applied during corona poling in order to reduce the coercive electric field (ferroelectric) or to approach the glass-transition temperature (T_g) of the material (NLO polymers). However, a thermal treatment during corona poling influences the charge trapping of the inner surfaces of the voids in ferroelectrets. The charge trapping in shallow traps is suppressed at elevated temperatures, leading to a higher ratio of charges in deep traps to those in shallow traps. Therefore, corona poling at elevated temperatures can improve the thermal stability of the internally charged macroscopic dipoles and hence the piezoelectricity of ferroelectres.[66] As already discussed in Ref. 1, corona poling through a grounded metal mask is suitable for producing periodic polarization patterns in a polymer film.

2. Poling with patterned electrodes

Another commonly used poling technique to pole piezo-, pyro-, and ferroelectric polymer electrets is electrode poling with an electric field larger than the coercive field of the film. Basically, there are three ways to generate patterned electrodes: (i) the electrode can be directly deposited onto the sample surface in the desired pattern, (ii) after deposition, a uniform electrode can be patterned by means of lithography and etching, or (iii) a patterned electrode can be fabricated independently and then brought into contact with the sample. The first two approaches may be useful for a variety of applications such as focusing ultrasound generators and receivers or quasiphase-matched second-harmonic generation (QPM-SHG), in which the patterned electrodes are sometimes also required for transducer operation. As already discussed in the earlier review,[1] large periodic deformations of the polymer film surface are caused by the electrostatic forces during poling and by the resulting viscous flow of the polymer in its rubbery state. These effects are usually detrimental but may be minimized by employing periodic poling electrodes on the substrate surface and a large-area continuous electrode on top of the polymer system.[1] Later studies indicated that the width and separation distance of the electrodes must be carefully designed in order to optimize the QPM efficiency.[67–69] The effective nonlinearity contrast can be optimized in ridge-waveguide structures.[70,71]

Patterned electrodes were also used in connection with thermal-pulse tomography (TPT) of ferroelectric polymers. High-resolution 3D polarization mapping of PVDF and P(VDF-TrFE) films poled with well-defined electrode gratings was realized by means of TPT.[72–74] As can be seen from Fig. 9, the polarization profiles reproduce the pattern of the electrode grating very well. In addition, a partial depolarization is observed in particular near the electroded surface. The TPT technique has close relevance to the topic of this paper,

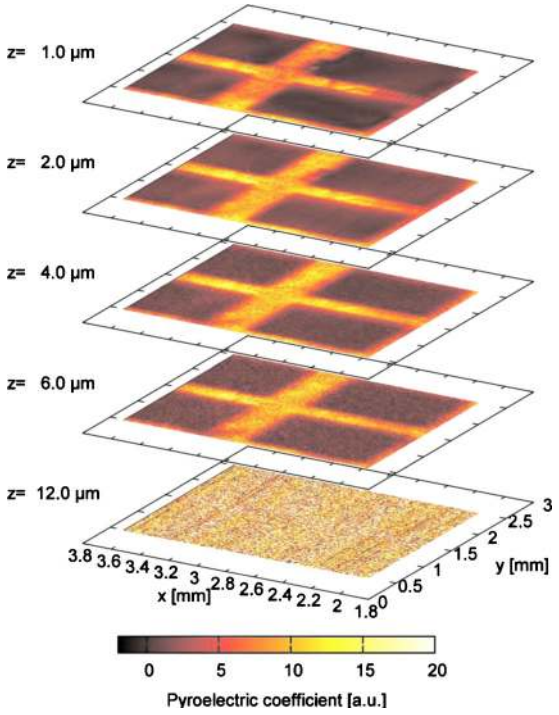

FIG. 9. (Color online) High-resolution 3D polarization map of a P(VDF-TrFE) sample poled with an electrode grating. Details of the electrode grating are very well reproduced (Ref. 74).

since it provides an efficient way to detect the patterned polarization achieved in piezo-, pyro-, and ferroelectric polymer electrets.[75]

Planar optical waveguides can be fabricated by means of electrical microcontact printing (E-μCP), in which the electrode has been implemented through the last of the above-mentioned approaches.[47,48,76,77] A stamp with a suitable pattern, usually prepared from elastomeric poly(dimethylsiloxane) (PDMS) and coated with a thin gold film, is placed in conformal contact with a dielectric film supported on a second electrode. A voltage is applied between the gold layer on the PDMS and the second electrode behind the dielectric film. The resultant current flows predominantly within the intimately contacted regions defined by the stamp pattern and bleaches the chromophores doped in these regions, leading to a change in the local index of refraction of the chromophore-doped polymer. By use of this technique, thin-film waveguides can be patterned in less than 90 s over large areas (more than 1 cm^2).

3. Electron-beam poling

In electron-beam poling, the sample is charged by an essentially monoenergetic electron beam in the range between a few and tens of kiloelectron volt. Depending on the electric-field distribution inside the sample, a well-confined space-charge layer is generated, the depth of which depends on the energy of the electron beam. In compact polymers, this dependence is usually given by a power law[78]

$$r = r_0\left(\frac{E_B}{E_0}\right)^n, \tag{18}$$

where E_B is the electron-beam energy, r_0 (in μm), E_0 (in keV), and n are constants to be determined from the experimental data. Electron-beam poling of ferroelectrets has also been reported.[61] With the difference that the near-surface charges are injected by means of an electron beam, the high electric field across the voids and the resulting internal breakdown are the same as with corona poling. Eletron-beam poling is suitable for patterning piezo-, pyro-, and ferroelectric polymer electrets along both the thickness and the in-plane directions.[1] It should be noted, however, that chemical modifications and some degradation of the material in the irradiated region are usually observed, which—at least in some cases—limits the applicability of electron-beam poling.[78,79]

However, the chemical modification and degradation of the material during electron-beam irradiation may be utilized for patterning in the case of chromophore-doped NLO polymers. These effects may occur with the chromophores within the host polymer. It is found that the chromophores are destroyed, and hence the second-order nonlinearity is erased by electron-beam exposure above a certain dose, while at very low radiation doses, no chromophore destruction is observed.[80] Chemical modification and degradation may also act on the polymer matrix. Electron-beam irradiation of poly(methyl methacrylate) (PMMA) above a certain dose leads to depolymerization of its main chain. The depolymerized layers are completely soluble when the irradiated sample is

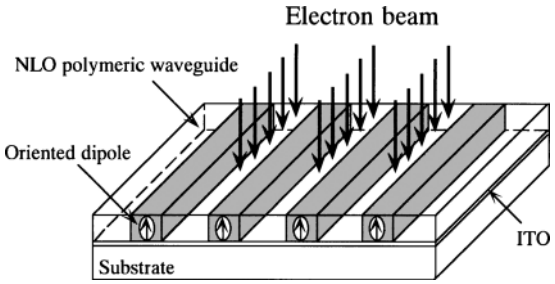

FIG. 10. Geometry of a periodically poled NLO polymer waveguide fabricated by electron-beam irradiation. The sample, spin-coated on a glass slide with a transparent ITO electrode, is irradiated by means of an electron-beam lithography system. The electron-beam irradiation is used to erase the microscopic hyperpolarizability of the chromophores within the exposed area. It may also be used to depolymerize the host polymer or to modify its T_g within the exposed area, allowing the fabrication of ridge-type optical channel waveguides of high quality in a corona or a two-step poling process (Ref. 80).

treated in isoamyl acetate with ethyl acetate and rinsed with pure water.[80,81] Corona poling is employed after the treatment in order to align the dipoles in the nontreated regions. On a chromophore-doped poly(4,4′-isopropylidenediphenylene terephthalate) copolymer (U-100), the irradiated areas could be removed by means of a thermal development after the electron-beam irradiation.[82,83] Unlike the wet development of PMMA, corona poling can be carried out simultaneously with the thermal development. When polystyrene (PS) is used as the host polymer, the T_g of the polymer is increased within the exposed area due to the cross-linking caused by the electron-beam irradiation, so that a domain-inversion structure can be generated by means of a two-step poling process (to be discussed later).[83] Based on the above-discussed mechanisms, a ridge-type optical channel waveguide with a high-quality pattern can be obtained by electron-beam irradiation with a suitable arrangement, as schematically shown in Fig. 10. This simple technique is applicable to various types of polymer film for implementing submicrometer patterns with high resolution.[84,85]

4. Photorelated poling

As already mentioned above, a simultaneous thermal treatment is often applied during the poling of ferroelectric and NLO polymers in order to enhance the mobility of the dipoles. The thermal treatment can be implemented by means of irradiation of the polymer with light. Using a focused laser beam, the temperature of the sample is increased mainly locally, thus allowing selective poling under a simultaneously applied electric field with suitable waveforms. In order to produce a waveguide with high performance, appropriate laser-beam wavelengths should be selected so that the film can be heated uniformly throughout its thickness. In addition, optimal values of the laser power, of the laser-beam diameter, of the speed of the moving stage, and of the electric-field strength are essential.[86]

Since the T_g of a ferroelectric PVDF film is well below room temperature (RT), the photothermal poling technique used on NLO polymer films is not suitable for patterning PVDF films. However, poled β-phase PVDF films can be locally depolarized by means of selective heat absorption

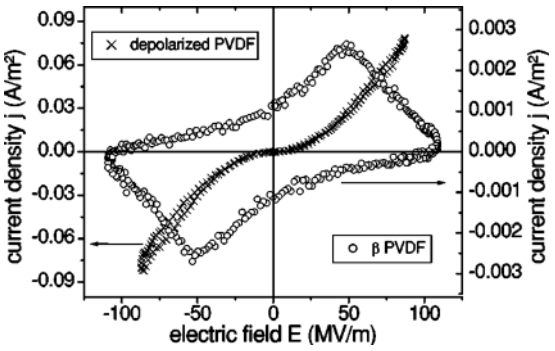

FIG. 11. Poling-field dependence (under a sinusoidal electric field at a frequency of 3 mHz) of the current density during poling of a depolarized PVDF film (left axis) in comparison to a β-phase PVDF film. The depolarization was achieved by controlled scanning of the top sample electrode with a focused laser beam (Ref. 87).

during controlled scanning of a focused laser beam across their top electrodes.[87] With the right processing parameters, an irreversible phase transformation from the β phase to a much less polar phase (α or α_p) occurs throughout the thickness of the poled β-phase PVDF films, without destruction of the film. Figure 11 shows the charging behavior of the depolarized and undepolarized areas of the PVDF film. The current density through the depolarized area under a sinusoidal electric field at a frequency of 3 mHz does not show any peaks.[88] With this technique, depolarized stripes with widths down to 80 to 90 μm can be produced on a 23 μm thick β-PVDF film.

For chromophore-doped NLO polymers, the dipole mobility can be increased through a photoisomerization process. Most chromophore molecules used in NLO polymers contain double bonds around which the molecules undergo a reversible so-called *trans-cis* transformation when they absorb light of a suitable wavelength, leading to a change in the shape of the dipolar molecule and an increase in its mobility.[9–12] Consequently, the molecular dipoles can sometimes be oriented by means of a simultaneously applied electric field even well below the T_g of the respective NLO polymer (photoinduced orientation, PIO), while light irradiation alone can destroy any previous orientation (photoinduced deorientation or depoling, PID).

Combined with appropriately designed schemes of electric field application, both PIO and PID can be employed to pattern the dipole polarization in NLO polymers.[89–92] Most recently, a new efficient approach was proposed for PIO patterning by means of scanning-probe microscopy.[93] The probe acts both as an electrode for applying an electric field [atomic force microscopy (AFM)] and as a sensor for detecting the polarization *in situ* [electrostatic force microscopy (EFM)]. Both, dipole orientation and contact electrification (CE) can occur during the interaction between probe and sample surface, generating heterocharges and homocharges, respectively. However, the CE effect is negligible if the AFM is operated in the tapping mode, which reduces the friction force and the time period of physical contact during poling. Figure 12(a) shows the fundamental principle: the dipoles are oriented by the electric field from the probe across the sample. In combination with illumination by a linearly polarized diode-pumped solid-state laser [Fig. 12(b)], dipole polarization is generated or erased locally.[93]

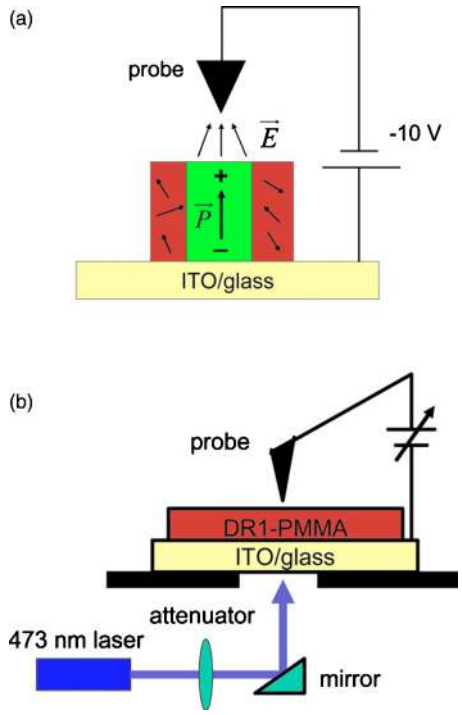

FIG. 12. (Color online) (a) Schematic view of the relationship between the probe bias and the dipole polarization/bound charges resulting from local poling with a negatively biased probe. (b) Selective PIO/PID during illumination with a laser source from the rear side (Ref. 93).

Photoinduced poling (PIP) still requires the presence of a dc electric field, while in all-optical poling (AOP) only light fields are involved.[94–96] During AOP, a polymer film is irradiated simultaneously by two superimposed coherent beams, one at frequency ω and the other at frequency 2ω. Under these conditions, the average of the cubic power of $\langle E^3 \rangle$ is nonzero (although the mean electric field $\langle E \rangle = \langle E_\omega + E_{2\omega} \rangle$ is zero), which results in selective polar excitation of the molecules. This technique allows for the orientation not only of dipolar molecules but also of molecules exhibiting octupolar symmetry.[97] Although only light fields are involved in AOP, an induced second-order susceptibility as high as that achieved by means of electric-field poling was obtained by optimizing the seeding conditions.[98,99] In order to optimize the charging efficiency, an appropriate intensity ratio of the two seeding beams is required, and the trade-off between the optical seeding efficiency and the transparency of the polymer should be taken into account.[100–104]

Advantages of patterning by means of PIP are the feasibility of generating complex patterns for integrated circuits and devices through appropriate masks and the good repeatability of the process. Whereas AOP is a promising technique that can be applied for the fabrication of photonic devices also with several advantages: The molecular-dipole orientation has a period exactly satisfying the phase-matching conditions for SHG, there is no need for poling electrodes, and patterning for optimal SHG can be easily achieved by scanning the focal area across the sample surface in a well-controlled manner. In addition, both PIP and AOP permit the

absence of thermal degradation of the chromophores that would be unavoidable during thermal poling at high temperatures. Unfortunately, the dipole orientation induced by PIP and AOP has a inferior thermal stability compared to thermal poling.[105,106] However, the stability of the orientation can be improved by means of a suitable thermal treatment under an applied field (PIP) or during seeding (AOP).[107–110] Another efficient way to improve the temporal stability of the orientation is using side-chain polymers with high T_g or thermally crosslinkable polymer systems as polymer matrices.[111–115]

5. Suitable combinations of poling techniques

Suitable combinations of different poling techniques may be utilized to generate highly special and more complicated polarization patterns. One example is the combination of poling with patterned electrodes and corona poling reported by Jung and Kinoshita.[116] In their study, a periodic electrode on a NLO polymer film is prepared by means of photolithography of a continuous aluminum layer, while a uniform indium-tin-oxide (ITO) layer is used as the second electrode. First, the dipoles underneath the patterned aluminum electrode are oriented by means of electrode poling. Then both the patterned aluminum electrode and the ITO electrode are grounded and corona poling is used to orient the dipoles within the remaining areas in the opposite direction. With this technique, a periodically domain-inverted poled-polymer waveguide for QPM-SHG can be fabricated.

Bimorph or multimorph polarization can be achieved in NLO polymer films through the combination of thermal poling and PIP. First, the whole film is uniformly poled by means of thermal poling, and afterwards, selective poling is achieved with PIP which reorients the dipoles only within the penetration depth of the irradiated light under an electric field opposite to that of the first poling step.

Two-step poling is proposed to prepare bimorph polarization in double layers of two ferroelectric or amorphous polymers with two different Curie or glass-transition temperatures.[44] With proper poling schemes, it is also possible to separately polarize different components within a sample. Rollik *et al.*[117] investigated the contributions of the crystalline and the amorphous phases, as well as the interface between them to the pyroelectricity of PVDF by selecting appropriate poling temperatures below and/or above T_g as well as poling fields lower and/or higher than the coercive field. In a semicrystalline ferroelectric polymer such as PVDF, there are three possible types of polarization, namely in the crystalline phase, in the amorphous phase, and at the crystalline-amorphous interface (Maxwell–Wagner or interface-charge polarization, MWI polarization). In a special strategy for selective and combined poling of these three contributions, the crystalline phase is poled with an electric field E_{PC} higher than the coercive field (for PVDF, $E_C > 80$ MV/m at RT). After this first poling step, all three kinds of polarization may be found in the polymer film. Then the sample is cooled down below T_g (for PVDF, $T_g \approx -42$ °C). The polarization of the amorphous phase can be erased if the electrodes are short-circuited before the temperature drops to T_g. The polarization of the amorphous phase can also be induced parallel ($E_{PA} < E_C$ with the same sign as E_{PC} during cooling) or antiparallel ($E_{PA} < E_C$ opposite to E_{PC} during cooling, as shown in Fig. 13) to that of the crystalline phase. If the sample is solely poled with E_{PA} and the electrodes are short-circuited before the temperature drops below T_g, only the MWI polarization is present after poling.

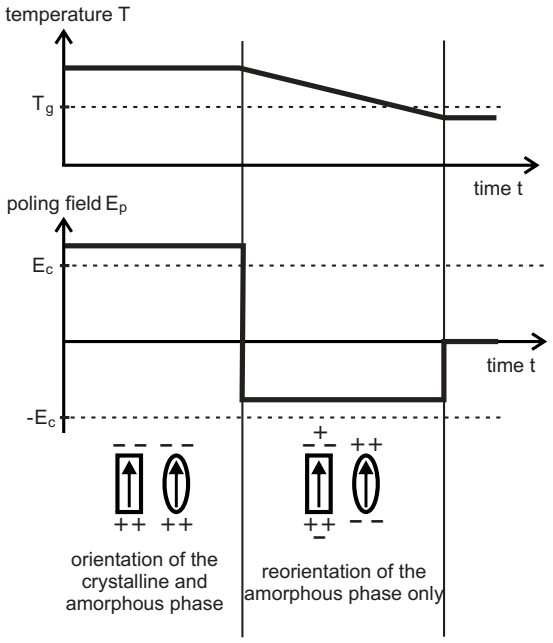

FIG. 13. Selective poling schemes for polar semicrystalline ferroelectric polymers. The resultant polarization of the amorphous phase is in antiparallel with that of the crystalline phase (Ref. 117).

In the case of ferroelectric composites of ceramic nanoparticles in a ferroelectric polymer matrix, the orientation of the polarization in the two components can be poled to be either parallel or antiparallel by means of a similar two-step poling techinique.[118,119] It is known that the pyroelectric coefficients p_3 of perovskite ceramics and ferroelectric polymers have the same sign (both negative), while the piezoelectric d_{33} coefficients have opposite sign (positive and negative for ceramics and ferroelectric polymers, respectively) because of the difference between primary and secondary (i.e., dipole-density) piezoelectricity, respectively. Thus, polymer-ceramic composites with enhanced pyroelectricity but greatly reduced piezoelectricity (when the orientation of the polarization in the two constituents is parallel) or vice versa (when the orientation of the polarization is antiparallel) can be obtained.[119,120] Such composites are of much interest for sensor applications, since a strong influence of temperature changes (or mechanical vibration) on a piezoelectric (respectively, pyroelectric) sensor can be avoided.[120,121]

B. Direct patterning

As already mentioned, patterned piezo-, pyro-, and ferroelectricity in poled polymer electrets may also originate from patterned sample structures, although poling is always necessary for rendering these polymer electrets electroactive. Conventional techniques for patterning polymer films in-

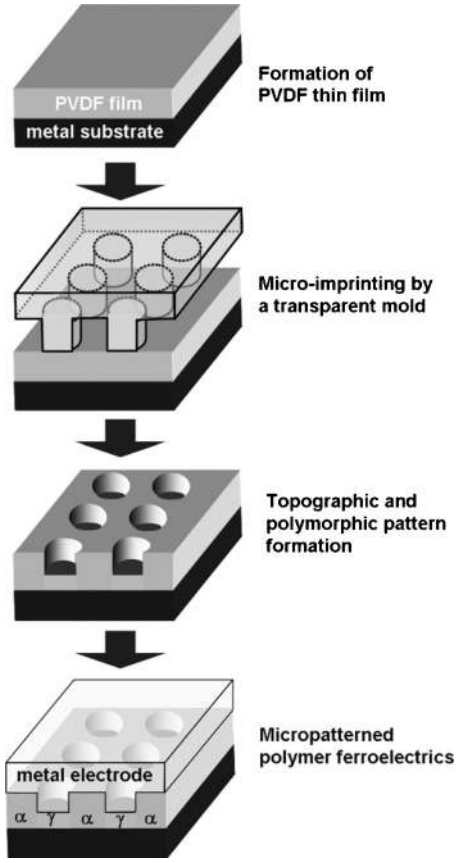

FIG. 14. A schematic view of the fabrication of micropatterned PVDF ferroelectrics. The localized pressure applied in microimprinting lithography leads to a polymorphic transition from the nonpolar α phase to the ferroelectric γ phase (Ref. 126).

clude laser ablation, numerically controlled drilling or punching, wet etching (with chemicals), dry etching (by means of plasma or reactive-ion etching), hot embossing lithography, photolithography, etc.[122] In this subsection, methods suitable for patterning the sample structure of piezo-, pyro-, and ferroelectric polymer films are discussed.

1. Direct patterning of single-layer polymer-electret films

It has been demonstrated that the crystallization of PVDF depends significantly on the hydrostatic pressure applied and that a pressure higher than 500 MPa, combined with specific thermal treatment, can yield a polar crystalline form in PVDF films that can be up to hundreds of micrometers thick.[123–125] Kang *et al.*[126] prepared patterned arrays of isolated ferroelectric γ-type domains embedded in the nonpolar α phase of thin PVDF films by means of microimprinting of a spin-cast α-type PVDF film. The thin PVDF film was melted and recrystallized after spin-casting in order to eliminate its initial surface roughness. Then a transparent elastic mold fabricated from PDMS with a topographic array pattern was compressed uniaxially onto the film for (sub)micrometer scale patterning, as shown in Fig. 14. This technique was also used to pattern β-phase ferroelectric P(VDF-TrFE) copolymer films. It is found that the remnant polarization of the P(VDF-TrFE) sample is dramatically enhanced by imprinting at a suitable temperature due to the increased crystallinity of the film. Various patterns have been created with good pattern transfer from the imprinting molds to the polymer films.[127] Nonlinear surface relief grating (SRG) in NLO polymer film was obtained by means of a simple technique using simultaneous process of emboss heating and thermal poling. In this case, a pressure-induced phase transformation does not occur. For master grating fabrication, a PI film with high thermal stability and high mechanical strength was prepared onto a metal plate and then the desired pattern on the PI film was achieved by a holographic method. The master grating was stamped under pressure into the NLO polymer at elevated temperature and a high voltage was applied between the metal plate and the ground. The film was cooled down with the pressure and the electric field and finally the master grating was removed. This simple technique is applicable to most of the NLO polymer films with short process time and low cost.[128]

Another patterning method that also relies on a PDMS mold is micromolding in capillaries (MIMIC).[129–131] In MIMIC, a PDMS stamp with a suitable surface-relief structure is conformally laid onto the substrate, thus, generating a network of capillaries between the two layers. A liquid prepolymer is sucked into this network by capillary action. Micropatterning of a semicrystalline PVDF solution was performed by means of temperature-controlled MIMIC.[132] O_2-plasma-treated PDMS molds with micrometer-scale relief features in their surfaces were conformally pressed onto the surface of polished single crystal silicon wafers, which were in turn placed on a temperature-controlled metal substrate. The polar solvent dimethylformamide was used because it produced predominantly γ-phase PVDF crystals and showed almost no swelling of PDMS. The PVDF solution injected into the inlets of the PDMS channels drenched rapidly to the outlet of PDMS due to capillary force and filled the interconnected channels between the molds and the substrates. After the solvent has fully evaporated, the PDMS stamp can be easily separated from the patterned microstructures because of its very low interfacial free energy. Well-defined micropatterns of PVDF were generated during fast directional evaporation at 120 °C.

It is well known that PVDF undergoes dehydrofluorination upon irradiation with x-rays, excimer lasers or ion beams.[133–140] These irradiation effects bring new possibilities of patterning. Morikawa *et al.* reported direct pattern transfer onto PVDF using x-ray photons from a synchrotron radiation source.[141,142] In this technique, a PVDF film is exposed to x-rays through an absorbing mask with the desired pattern. As a result of the photodegradation, a maximum etch depth of more than 9 μm is achieved within the exposed area, thus, transferring the pattern into the PVDF film. *In situ* mass spectrometry reveals that the major degradation process is dehydrofluorination, while no carbon-containing species are detected. The photoemission spectra, in combination with *ab initio* molecular-orbital calculations, indicate the formation of fully conjugated C=C double bonds during photodegradation of the polymer. Therefore, the main effects of the photodegradation in PVDF seem to be the shrinking of the irradiated polymer region because of dehydrofluorination and the generation of conjugated bonds. The technique is

also used to directly pattern very thin P(VDF-TrFE) films.[143] A nickel wire-mesh mask is employed for patterning. The residual material within the exposed region is carbon rich because of the formation of double bonds in the polymer chain and crosslinking between chains. In contrast to the case of pure PVDF, the main photofragments include carbon-containing species such as CHF, CH_2, and CF_2, which is attributed to the presence of the TrFE monomer species.

Various patterned structures in chromophore-doped NLO polymers can be achieved through photobleaching and photoablation induced by selective light irradiation. As mentioned above, under irradiation at a suitable wavelength, a reversible *trans-cis* photoisomerization occurs in chromophore molecules. However, under irradiation with an energy density higher than that required for photoisomerization, an irreversible photobleaching occurs, during which the double bonds in the chromophores are broken and their nonlinearity is easily erased.[144–147] Thus, patterning can be done by locally bleaching the chromophores with such irradiation through a suitable photomask, while poling of the nonbleached areas can be carried out before or after the photobleaching. In the case of chromophore-doped NLO polymers based on photopolymerizable resins, photopatterning takes place mostly in the polymer matrix.[148,149] The polymerization process induced by an exposure to visible light hardens the initially soft matrix material and freezes the orientation of the chromophore molecules. After irradiation with a periodic illumination pattern, the film was charged in a static electric field. The chromophores within the nonpolymerized zones were oriented along the poling field, while those in previously polymerized areas remained oriented at random. Thus, a periodic polarization structure defined by the illumination pattern was created.

A photomechanical effect associated with the photoisomerization of azochromophores is identified and used to pattern NLO polymers.[12,150–152] The isomerization process generates pressure in the polymer matrix and thus also a localized photomechanical deformation of the material. There is a crossover temperature (normally much lower than T_g), below and above which photoexpansion and photocontraction are observed, respectively. For patterning, the sample is illuminated with a sinusoidal light intensity (or polarization) pattern generated by two coherent laser beams. Patterning can be realized by either photoexpansion or photocontraction, where the pattern phase is in opposite in the two cases. A sinusoidal grating (SRG) without any defects is obtained on the film surface with a depth of hundreds of nanometers.[151]

For most NLO polymer films, such a spontaneous surface patterning occurs already at relatively low laser powers up to a saturation value without destructive ablation. The resulting SRG can be erased by heating the sample above T_g. However, laser irradiation at much higher energy density leads to photoablation of NLO polymer films. Laser ablation of polymers is an established technique in the electronic industry.[153] The photoablation of NLO polymers is due to the evaporation of the material and the ablation depth is proportional to the irradiation energy.[147,154–156] The SRG fabricated through photoablation is thermally stable up to a temperature higher than the T_g of the polymer. Figure 15 shows the surface profile of a typical SRG on a urethane-urea copolymer observed by means of AFM. By means of laser interferometry, the grating period can be adjusted from a submicrometer to a millimeter scale by adjusting the incidence angle between the two writing beams.

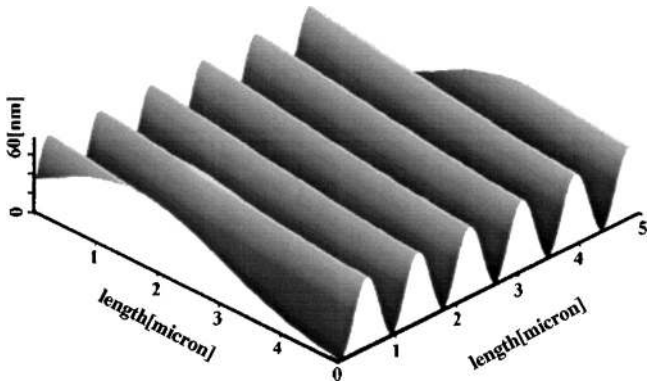

FIG. 15. AFM surface profile of a grating on a urethane-urea copolymer developed by laser interferometry. After fabrication, the grating was heat-treated for 60 min at 150 °C, i.e., above the T_g (141 °C) of the copolymer (Ref. 155).

2. Patterned layer structures

Very often, bi- or multilayer structures exhibit useful additional functions that are not possible with any of the constituents alone. The above-discussed double-layer structures of ferroelectric or amorphous polymers with two different T_c or T_g parameters are typical examples. These layer structures were, however, included in Sec. III B 2, since the implementation of their functions requires specifically designed poling schemes. A double-layer system that consists of an amorphous fluoropolymer (Teflon-AF) film plus a NLO polymer film was proposed in order to improve the polarization stability in the NLO polymer. The stack was corona poled from the Teflon-AF side so that the dipole orientation in the NLO polymer can be stabilized by the electric field from the space charge in the Teflon-AF layer. Because Teflon-AF can provide very good thermal stability of the space charge, the stability of the dipole polarization and hence also of the NLO effects in the double-layer system is significantly improved in comparison to a single film of the same NLO polymer.[157]

Multilayer ferroelectric polymer stacks are designed and prepared in order to improve the sensitivity of the resulting transducers. Ferroelectric polymer stacks are widely used in ultrasonic transducers. In the case of folded multilayer structures, the ferroelectric polarizations of adjacent layers have opposite signs and are oriented along the thickness direction. The electrodes of folded structures are also alternating so that all even-numbered and all odd-numbered electrodes are connected together, respectively. For an actuator, the output amplitudes of the individual layers are added, while both the resonance frequency and the electrical impedance are reduced in comparison to an individual layer.[158,159] The resonance frequency of the multilayer stack can be adjusted by choosing the thickness of each single layer.[160] In order to obtain a bandwidth comparable to that of a single layer, a

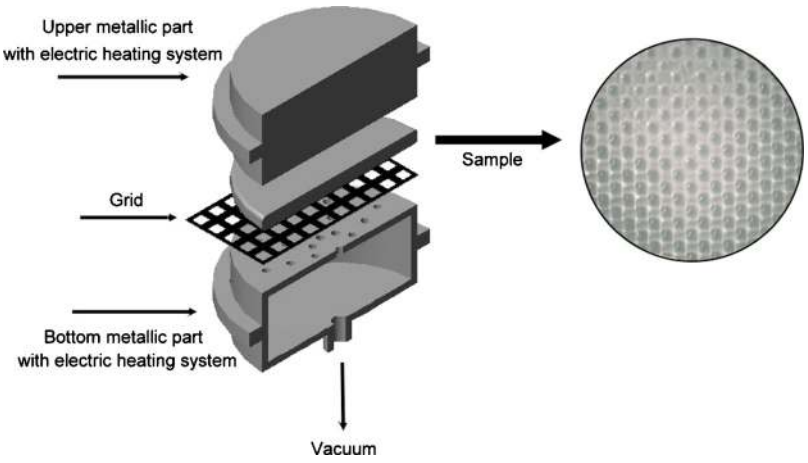

FIG. 16. (Color online) Schematic view of the setup for preparation of thermoformed bubble structures between two polymer films (Ref. 176).

switchable Barker-code stack design is adopted in which the electrodes of the transducer can be connected in parallel or in series for the transmitting and the receiving mode, respectively.[158,161]

Recently, miniaturized monolithic multilayer cantilevers were fabricated from P(VDF-TrFE) on a substrate by means of alternating spin-coating and electrode-evaporation processes. In the multilayer structures, polymer layers with a thickness of several micrometers are separated by aluminum electrodes with a thickness of hundreds of nanometer. After cutting the stack with a dicing saw or etching with an inductively coupled plasma, the internal electrodes of the multilayer structure are exposed, which allows for the electrical connection of alternate electrodes. An actuator consisting of three multilayered P(VDF-TrFE) cantilevers was fabricated. It shows high performance with respect to force, deflection, and motion even at relatively low driving voltages.[162–164]

Layer sandwiches of space-charge polymer-electret films were already used in early implementations of piezoelectrets. Kacprzyk *et al.*[165–167] reported piezoelectric double-layer sandwiches of one softer and one harder layer with electret charges in between and confirmed the possibility of making piezo- or ferroelectrets in this way. Porous polytetrafluoroethylene (PTFE) is very attractive for use as piezoelectric transducer material in such hard/soft electret sandwiches, because of high surface-charge stability and softness.[168–171] Fluoropolymer ferroelectrets were produced by sandwiching a highly porous PTFE [so-called expanded PTFE (ePTFE) consisting of 91% air and 9% fibrous PTFE] between two solid fluoroethylenepropylene (FEP) layers.[172,173] The FEP layers form structurally and electrically dense layers, whereas the fibrous ePTFE layer keeps the two FEP layers apart, forming air-filled cavities. Upon corona charging, breakdown occurs within the cavities when the electric field strength exceeds the Paschen-breakdown threshold value of air. Charges of both polarities are separated during plasma formation and some of them are trapped on the internal surfaces of the top and bottom FEP layers. After bipolar charging of their internal surfaces, the cavities can be considered as macroscopic dipoles. The piezoelectric d_{33} coefficient is thermally stable if the sample is charged at elevated temperatures. However, d_{33} decays from 800 to 400 pC/N under atmospheric pressures within six days, and repeated mechanical loading leads to a similar loss of piezoelectricity, apparently related to mechanical fatigue in the highly porous ePTFE.

For industrial applications, ferroelectrets with well-controlled distributions or even uniform values of void size and void shape and with good thermal stability of the piezoelectricity are very desirable. Such ferroelectrets may be easily produced on a large scale with good reproducibility and they also promise long lifetimes. Several strategies were proposed for preparing ferroelectrets of this kind. A stack of two FEP films was placed between two cylindrical metal plates which can be independently heated. One plate is completely solid, while the other one has tiny holes that are connected to a vacuum pump. An additional metal grid was placed between the stack of FEP films and the bottom plate. Most of the air was removed through the holes of the bottom plate by means of the vacuum pump and the adjacent FEP film was sucked into the openings of the metal grid. By heating and pressing the upper plate onto the stack, air cavities with the same diameter as the grid openings were created.[174–176] Figure 16 schematically shows the setup and the preparation procedure. After corona charging, novel piezo- or ferroelectrets with regular arrays of millimeter-sized dome-shaped bubbles between Teflon-FEP films had been generated.

More recently, this method was modified and further improved by Zhang *et al.*[177] In their study, a metal mesh with (sub)millimeter spacing was pressed on stacks of alternating FEP and PTFE films. With proper thermal treatment, the polymer layers were fused underneath the wires of the metal mesh and cavities were formed between the fused areas because of the thermally expanding trapped air and the thermal softening of the fluoropolymer films. In the ferroelectrets thus obtained, strong piezoelectricity is measured only within the highly compressible areas of the air-filled cavities. Thus, large variations in the piezoelectricity are observed across the sample surface. Nevertheless, such structures are very attractive for applications in piezoelectric sensors and actuators, since active areas of at least several square millimeter are usually available, and also, since averaging of the piezoelectric d_{33} coefficient can often be exploited.

The aforementioned techniques for fabricating ferroelectrets suffer, however, from the difficulties of processing

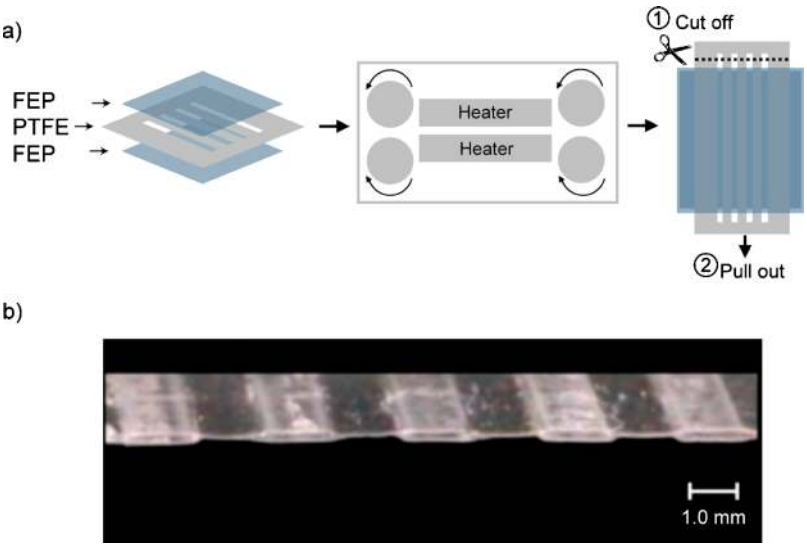

FIG. 17. (Color online) (a) Schematic view of the preparation process for tubular-channel ferroelectrets. A sandwich consisting of two solid FEP films with a well-designed PTFE template between them is laminated at 300 °C. After lamination, the stack is cooled down to RT. An FEP system with open channels is obtained after removing the non-sticking PTFE template from the stack. (b) Optical micrograph of the cross section of a sample together with one of its surfaces (which is seen because of a small angle between sample surface and illuminating light (Ref. 178).

and/or of melting the soft and hard layers. Very recently, FEP ferroelectrets with well-controlled and uniform voids have been produced by a straightforward lamination process.[178] The preparation setup is based on a lamination device with a suitable temperature controller. For sample preparation, a PTFE template consisting of several well-cut stripes with clearly defined and evenly distributed openings between them is sandwiched between two solid films of Teflon FEP. The three-layer sandwich is fed to the lamination machine, whose operating temperature was set to 300 °C. This temperature is chosen, since it is substantially higher than the melting temperature of FEP (about 260 °C) but still well below the melting point of PTFE at 327 °C. After lamination, the stack is naturally cooled down under laboratory conditions so that the two FEP layers are intimately bonded to each other through the openings in the PTFE template. A cellular FEP structure with tubular voids is obtained after removal of the PTFE template. Figure 17(a) schematically illustrates the preparation, while a typical cross section of the resulting layer system is shown in Fig. 17(b). With this novel technique that may also be adapted to continuous roll-to-roll processing, it is possible to create uniform channels with a large range of widths, heights, lengths, as well as arbitratry channel patterns.

When a voltage V is externally applied to such a two-layer FEP system, the electric field inside the tubular channels E_g is given by

$$V = E_g\left(\frac{d_p}{\varepsilon_p} + d_g\right), \tag{19}$$

where d_p is the combined thickness of the FEP layers, d_g is the internal void height, and $\varepsilon_p = 2.1$ is the dielectric permittivity of the solid FEP films. According to Townsend's model, the critical breakdown field of common gases in a uniform electric field is a function of gas pressure p and electrode spacing d (which in our case is equal to the internal void height)[179]

$$E_C = \frac{Ap}{B + \ln(pd)}, \tag{20}$$

where the constant B is given by

$$B = \ln\left[\frac{C}{\ln(1 + 1/\gamma)}\right]. \tag{21}$$

For air, $A = 273.8$ V m^{-1} Pa^{-1} and $C = 11$ m^{-1} Pa^{-1} are experimentally determined constants and $\gamma = 0.01$ is the so-called second ionization coefficient. Uniform DBDs inside the tubular voids could be confirmed with images from an electron-multiplying charge-coupled-device camera with high sensitivity. It is observed that the threshold voltage for uniform DBDs is in very good agreement with the value calculated from Eqs. (19)–(21). During the DBDs, the inner top and bottom surfaces of the tubular voids were charged positively and negatively, respectively. In preliminary studies, a piezoelectric d_{33} coefficient of 160 pC/N was obtained. After charging at suitable elevated temperatures, the piezoelectricity is stable at temperatures up to at least 130 °C. The new technique has the obvious advantages of simplicity and of well-controlled void geometries and patterns. Furthermore, it can be easily adopted to continuous industrial fabrication.

IV. SELECTED APPLICATIONS

Patterning of piezo-, pyro-, and ferroelectric polymer electrets may either improve their piezo-, pyro-, and ferroelectricity, or lead to new functionalities for a range of innovative applications. In order to highlight the applications potential of patterned polymer electrets, several examples will be discussed in this section.

A very interesting application of ferroelectric polymers is in rewritable data-storage devices.[180–186] Recording of a binary optical image was achieved by means of AOP.[181] Either the ω beam or the 2ω beam may carry the image information. In order to obtain high polar order, an appropriate intensity ratio between the ω and the 2ω beams is required. The image written during AOP does not erase the optical information that was previously recorded by means of photo-

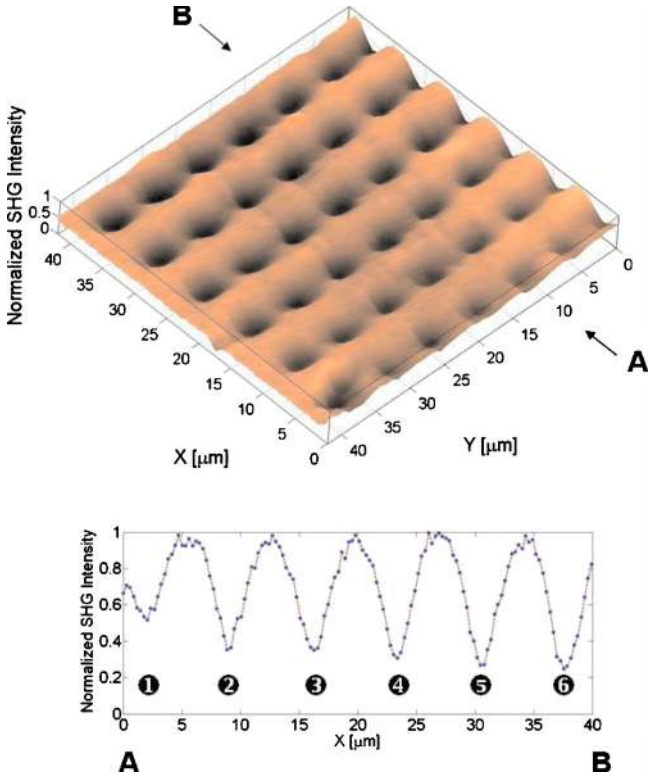

FIG. 18. (Color online) SHG image of the sample after PID recording of a pattern. Top: 3D tomography over an area of 40×40 μm^2. Bottom: SHG profile along a line from A to B across the sample, showing the change in SHG contrast at a constant mean power of 30 mW and for increments of 30 ms in irradiation time. The full width at half maximum of the holes is about 2.8 μm (Ref. 185).

induced birefringence or dichroism. Therefore, a rather large storage capability is available when the two methods are combined.[99] The localized loss in SHG efficiency during PID was also exploited for optical data storage.[185] A spin-coated film of PMMA grafted with 10% Disperse Red 1 (DR1) was first uniformly corona-poled and then put on an X-Y-Z-θ stage, which was placed in the focal point of a 50× objective lens from a microscope. The sample can be regularly repositioned by the XYZ stage, and a femtosecond-pulse near-IR laser source was used for local depoling. A 3D tomography of the SHG signal of the sample after the recording process is shown in the upper part of Fig. 18, while the lower part depicts a profile of the depth in the contrast across the SHG signal. Performed with appropriate intensities, a given patterned area can be imaged repeatedly without detectable losses in either contrast or resolution, indicating that this technique is suitable for a rewritable data storage device.

A simple device for focusing air-borne ultrasound was fabricated using a Fresnel zone plate (FZP) or a Fresnel phase plate (FPP) electrode pattern.[187,188] Figure 19 schematically shows an FZP electrode pattern on piezoelectric film which may be prepared by means of standard photolithography, while the other side of the film carries a continuous electrode. Since the acoustic signals are generated under the patterned electrodes only, the emitted ultrasonic radiation interferes at some points determined by the zone radii. The intensity and resolution of an FZP transducer can be improved by using an FPP pattern instead. In an FPP, alternate

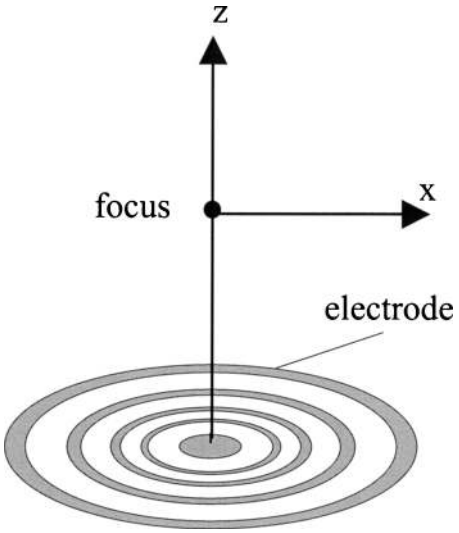

FIG. 19. Schematic view of a FZP for focusing ultrasound (Ref. 31).

zones are poled in opposite directions and both sides of the film are finally coated with continuous electrodes.[187]

Piezoelectric polymers are very suitable for such applications due to their low acoustic impedances that can be close to those of water or even air. For PVDF, the impedance match can be further improved with epoxy (or metal-loaded epoxy) backings. The focal-plane profile of the ultrasonic emission from an epoxy-backed three-zone FZP prepared with PVDF was found to be in good agreement with the theoretically predicted one.[188] Cellular PP ferroelectrets with an FZP electrode provide sound focusing even without any backing, again in excellent agreement with theoretical predictions from the Fresnel theory.[31,189] An accessible frequency of up to 1 MHz is sufficient for most applications in air-borne ultrasound.[31]

Layer structures can be very efficient for enhancing the sensitivity of ferroelectret-transducer devices. In early studies, micromovement actuators were manufactured with multilayer ferroelectret stacks in order to add the voltage-induced thickness variations in the individual films.[32,190] Sensitivity improvements of piezoelectric microphones from cellular polymer ferroelectrets were also achieved in this way.[191] Microphones consisting of a single well-prepared cellular PP ferroelectret typically have a sensitivity of about 2.2 mV/Pa and an equivalent noise level of 37 dB(A) at 1 kHz. A five-layer stacked PP ferroelectret microphone exhibited a sensitivity of approximately 10 mV/Pa and an equivalent noise level of 26 dB(A), well comparable to the respective values of traditional electret condenser microphones.[191] Figure 20 shows the frequency responses of microphones with one and with five cellular PP ferroelectrets, respectively. A flat frequency response is observed over the whole audio-frequency range. Unlike in electret condenser microphones, miniature air gaps are not necessary in ferroelectret microphones, allowing for a much simpler design. Additionally, the ferroelectret microphones have low harmonic distortion and high resonance frequencies. These features make such microphones very suitable for a wide range of applications.

Some applications require complex piezo-, pyro-, or fer-

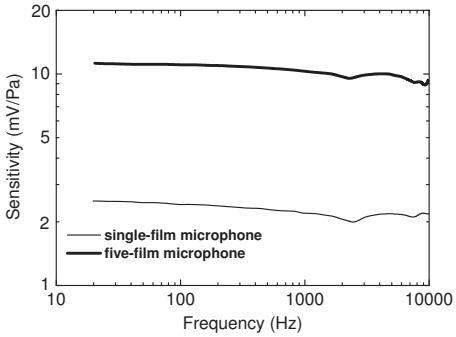

FIG. 20. Frequency response of cellular-PP piezoelectret microphones with a single film and with a stack of five films, determined by means of a comparison method in an acoustic coupler (Ref. 191)

roelectricity patterns which may be achieved by a suitable combination of different patterning techniques. Piezoelectric P(VDF-TrFE) films were patterned by means of a new mold-transfer technique in order to form novel dome and bump shapes. The resulting transducers were assembled on a microcatheter to yield flexible tactile sensors.[192] For sample preparation, a micromachined mold with domes (wells) on a micrometer-to-millimeter scale was fabricated. A piezoelectric polymer solution was spin-coated (screen-printed) onto the mold, followed by a suitable thermal treatment. Samples were deposited with patterned electrodes and dome- or bump-shaped piezoelectric tactile sensors were obtained after dc poling at elevated temperatures. Figure 21 schematically

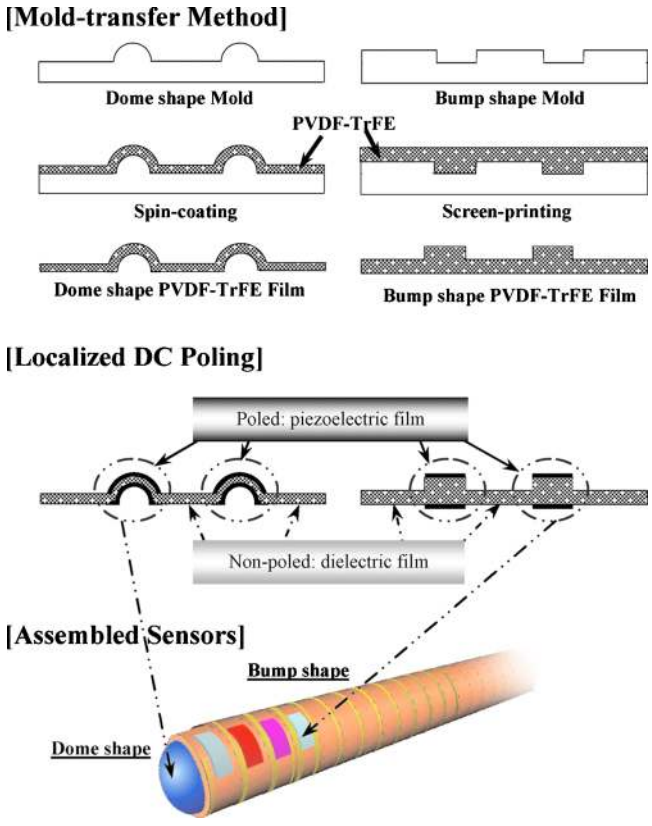

FIG. 21. (Color online) Schematic view of a new mold-transfer technique to pattern P(VDF-TrFE) films and of the new dome- and bump-shaped tactile-sensor modules for smart microcatheters which can detect forces as small as 25 mN and 40 mN, respectively (Ref. 192).

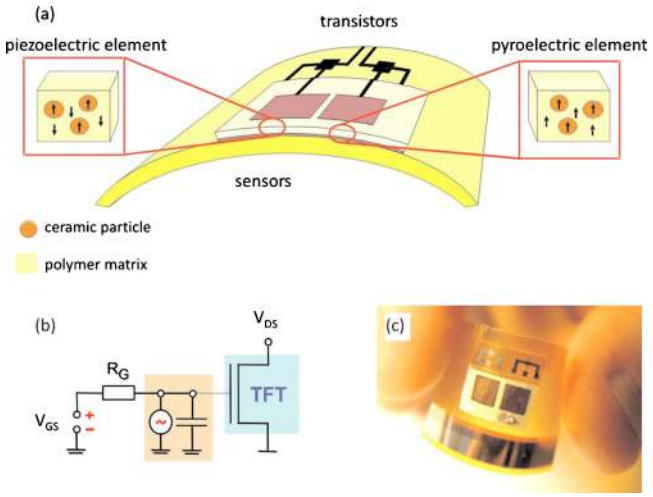

FIG. 22. (Color online) (a) Schematic view of a bifunctional sensor array where the flexible polymer-ceramic sensor frontplane is laminated onto a flexible transistor backplane. The piezoelectric subcell has an antiparallel orientation of the polarizations in the ceramic nanoparticles and the ferroelectric polymer matrix, while the pyroelectric subcell has a parallel orientation of the two polarizations. (b) The equivalent circuit for the subcells. (c) A digital photograph of the sensor prototype (Ref. 121).

shows this technique and a "smart" microcatheter with a dome-shaped piezoelectric film at its tip and a bump-shaped film array along its tube wall. Obviously, this technique represents a combination of direct patterning and patterning by selective poling. The tactile sensors were able to detect forces as small as 40 mN for the bump-shaped sensors and 25 mN for the dome-shaped sensors. The response of the sensors was very stable over a frequency range from 1 to 100 Hz and a temperature range from RT to 45 °C. The sensors are easy to fabricate, to miniaturize, and to pole selectively with standard microelectromechanical-systems technology. They may find numerous applications in micro-catheters or other miminally invasive biomedical devices.

Another example for the combination of direct patterning and patterning by selective poling was reported by Graz *et al.*[121] very recently. A bifunctional polymer-ceramic nanocomposite that can be used for either pressure or temperature sensing was prepared. Piezoelectric lead-titanate nanoparticles were dispersed in a ferroelectric P(VDF-TrFE) polymer matrix during sample preparation. Since the Curie temperature of lead titanate is higher than that of P(VDF-TrFE), the polarizations in the ceramic particles and in the ferroelectric polymer matrix can be oriented either parallel or antiparallel by means of an area-selective two-step poling sequence.[44] As already mentioned, the pyroelectric coefficients p_3 of lead titanate and P(VDF-TrFE) have the same sign, while the piezoelectric d_{33} coefficients have opposite sign. Therefore, proper parallel (antiparallel) orientation of the polarization leads to a vanishing piezoelectric (pyroelectric) effect and an enhanced pyroelectric (piezoelectric) effect.[121] Figure 22(a) schematically illustrates a bifunctional sensor cell, in which the subcell with an antiparallel orientation of the polarizations in the ceramic nanoparticles and in the ferroelectric polymer matrix is sensitive to pressure changes, while the other subcell with parallel orientation of the polarizations is sensitive to temperature variations. The

two subcells are laminated, respectively, to two transistors on the backplane. The equivalent circuit for the two sensor elements is shown in Fig. 22(b), and Fig. 22(c) represents a photographic image of a sensor prototype. The subcells essentially respond linearly to the input variables they are designed for and exhibit only small cross-talk.

V. CONCLUSION

Semicrystalline ferroelectric polymers, amorphous polymers containing chromophore molecules, and cellular polymer ferroelectrets belong to the family of electroactive polymers. They are attractive from both fundamental scientific and applications-oriented points of view, because of their significant piezo-, pyro-, and ferroelectricity, in combination with the intrinsic features of polymers such as low permittivity, low thermal conductivity, softness and flexibility, good acoustic impedance matching to air and water, relatively low cost, etc. Appropriate patterning of such materials may lead to improved or innovative macroscopic piezo-, pyro-, and ferroelectric or NLO properties and to devices that are useful for a range of applications. Special patterns may be achieved by means of suitable poling techniques and/or appropriate sample-preparation procedures. Various patterning techniques such as selective poling, including corona poling through a mask, poling with patterned electrodes, electron-beam poling, photothermal poling, AOP, PIP, as well as suitable combinations of poling techniques have been reviewed. Patterning of a single film or of layered structures by means of suitable sample-preparation procedures has been discussed, with special emphasis on new results from the author's team. Finally, a survey of selected applications is presented.

ACKNOWLEDGMENTS

The author gratefully acknowledges Dipl.-Ing. Werner Wirges (University of Potsdam, Germany), Professor Axel Mellinger (Central Michigan University, Mt. Pleasant, Michigan, USA), and Professor Siegfried Bauer (Johannes Kepler University, Linz, Austria) for many stimulating and fruitful discussions on the topics of this paper. He is particularly indebted to Professor Reimund Gerhard (University of Potsdam) for several useful suggestions and for a critical reading of the manuscript. Last, but not least, the author thanks the Deutsche Forschungsgemeinschaft (DFG) for providing a Research Fellowship (Reference No. QI 65/1-1) to him and the European Commission for co-funding some of the equipment used in his own work.

[1]S. Bauer, J. Appl. Phys. **80**, 5531 (1996).
[2]G. Eberle, H. Schmidt, and W. Eisenmenger, IEEE Trans. Dielectr. Electr. Insul. **3**, 624 (1996).
[3]G. M. Sessler, *Electrets*, 3rd ed. (Springer, New York, 1999).
[4]E. Fukada, IEEE Trans. Ultrason. Ferroelectr. Freq. Control **47**, 1277 (2000).
[5]V. V. Kochervinskiĭ, Crystallogr. Rep. **48**, 649 (2003).
[6]S. B. Lang and S. Muensit, Appl. Phys. A: Mater. Sci. Process. **85**, 125 (2006).
[7]E. Fukada, IEEE Trans. Dielectr. Electr. Insul. **13**, 1110 (2006).
[8]V. V. Kochervinskiĭ, Crystallogr. Rep. **54**, 1146 (2009) and references therein.
[9]M. Dumont and A. E. Osman, Chem. Phys. **245**, 437 (1999).
[10]A. Natansohn and P. Rochon, Chem. Rev. **102**, 4139 (2002).
[11]R. H. El Halabieh, O. Mermut, and C. J. Barrett, Pure Appl. Chem. **76**, 1445 (2004).
[12]K. G. Yager and C. J. Barrett, J. Photochem. Photobiol., A **182**, 250 (2006).
[13]J. A. Delaire and K. Nakatani, Chem. Rev. **100**, 1817 (2000).
[14]P. Günter, *Nonlinear Optical Effects and Materials* (Springer, New York, 2002).
[15]H. Ma, A. K. Y. Jen, and L. R. Dalton, Adv. Mater. (Weinheim, Ger.) **14**, 1339 (2002).
[16]F. Kajzar, K. S. Lee, and A. K. Y. Jen, Adv. Polym. Sci. **161**, 1 (2003).
[17]Y. V. Pereverzev, O. V. Prezhdo, and L. R. Dalton, ChemPhysChem **5**, 1821 (2004).
[18]S. K. Yesodha, C. K. S. Pillai, and N. Tsutsumi, Prog. Polym. Sci. **29**, 45 (2004).
[19]C. C. Chang, C. P. Chen, C. C. Chou, W. J. Kuo, and R. J. Jeng, J. Macromol. Sci., Polym. Rev. **45**, 125 (2005).
[20]H. Ma, S. Liu, J. Luo, S. Suresh, L. Liu, S. H. Kang, M. Haller, T. Sassa, L. R. Dalton, and A. K. Y. Jen, Adv. Funct. Mater. **12**, 565 (2002).
[21]M. J. Cho, D. H. Choi, P. A. Sullivan, A. J. P. Akelaitis, and L. R. Dalton, Prog. Polym. Sci. **33**, 1013 (2008).
[22]Y. Wada and R. Hayakawa, Jpn. J. Appl. Phys. **15**, 2041 (1976).
[23]J. J. Crosnier, F. Micheron, G. Dreyfus, and J. Lewiner, J. Appl. Phys. **47**, 4798 (1976).
[24]R. Gerhard-Multhaupt, IEEE Trans. Dielectr. Electr. Insul. **9**, 850 (2002).
[25]S. Bauer, R. Gerhard-Multhaupt, and G. M. Sessler, Phys. Today **57**(2), 37 (2004).
[26]M. Wegener and S. Bauer, ChemPhysChem **6**, 1014 (2005).
[27]S. Bauer, IEEE Trans. Dielectr. Electr. Insul. **13**, 953 (2006).
[28]M. Lindner, S. Bauer-Gogonea, S. Bauer, M. Paajanen, and J. Raukola, J. Appl. Phys. **91**, 5283 (2002).
[29]X. Qiu, A. Mellinger, M. Wegener, W. Wirges, and R. Gerhard, J. Appl. Phys. **101**, 104112 (2007).
[30]X. Qiu, A. Mellinger, W. Wirges, and R. Gerhard, Appl. Phys. Lett. **91**, 132905 (2007).
[31]M. Lindner, H. Hoislbauer, R. Schwödiauer, S. Bauer-Gogonea, and S. Bauer, IEEE Trans. Dielectr. Electr. Insul. **11**, 255 (2004).
[32]A. Savolainen and K. Kirjavainen, J. Macromol. Sci., Chem. **A26**, 583 (1989).
[33]M. Wegener, W. Wirges, and R. Gerhard-Multhaupt, Adv. Eng. Mater. **7**, 1128 (2005).
[34]W. Wirges, M. Wegener, O. Voronina, L. Zirkel, and R. Gerhard-Multhaupt, Adv. Funct. Mater. **17**, 324 (2007).
[35]P. Fang, M. Wegener, W. Wirges, R. Gerhard, and L. Zirkel, Appl. Phys. Lett. **90**, 192908 (2007).
[36]E. Saarimäki, M. Paajanen, A. M. Savijärvi, H. Minkkinen, M. Wegener, O. Voronina, R. Schulze, W. Wirges, and R. Gerhard-Multhaupt, IEEE Trans. Dielectr. Electr. Insul. **13**, 963 (2006).
[37]O. Voronina, M. Wegener, W. Wirges, R. Gerhard, L. Zirkel, and H. Münstedt, Appl. Phys. A: Mater. Sci. Process. **90**, 615 (2008).
[38]C. J. Dias and D. K. Das-Gupta, IEEE Trans. Dielectr. Electr. Insul. **3**, 706 (1996).
[39]A. K. Batra, M. D. Aggarwal, M. E. Edwards, and A. Bhalla, Ferroelectrics **366**, 84 (2008).
[40]S. F. Mendes, C. M. Costa, V. Sencadas, J. S. Nunes, P. Costa, R. Gregorio, Jr., and S. Lanceros-Méndez, Appl. Phys. A: Mater. Sci. Process. **96**, 899 (2009).
[41]D. A. van den Ende, B. F. Bory, W. A. Groen, and S. van der Zwaag, J. Appl. Phys. **107**, 024107 (2010).
[42]L. M. Ganesan, P. Frübing, A. Mellinger, and R. Gerhard, J. Phys. D: Appl. Phys. **42**, 092006 (2009).
[43]L. M. Ganesan, W. Wirges, A. Mellinger, and R. Gerhard, J. Phys. D: Appl. Phys. **43**, 015401 (2010).
[44]S. Bauer-Gogonea, S. Bauer, and R. Gerhard-Multhaupt, Braz. J. Phys. **29**, 306 (1999) and references therein.
[45]Y. Xia, J. A. Roger, K. E. Paul, and G. M. Whitesides, Chem. Rev. **99**, 1823 (1999).
[46]L. J. Guo, J. Phys. D: Appl. Phys. **37**, R123 (2004).
[47]A. P. Quist, E. Pavlovic, and S. Oscarsson, Anal. Bioanal. Chem. **381**, 591 (2005).
[48]B. D. Gates, Q. Xu, M. Stewart, D. Ryan, C. G. Willson, and G. M. Whitesides, Chem. Rev. **105**, 1171 (2005).
[49]C. Liu, Adv. Mater. (Weinheim, Ger.) **19**, 3783 (2007).
[50]D. A. Berlincourt, D. R. Currand, and H. Jaffe, in *Physical Acoustics*,

edited by W. P. Mason (Academic, New York, 1967) Vol. I, Pt. A.
[51]H Dvey-Aharon and P. L. Taylor, Ferroelectrics **33**, 103 (1981).
[52]X. Qiu, M. Wegener, W. Wirges, X. Zhang, J. Hillenbrand, Z. Xia, R. Gerhard-Multhaupt, and G. M. Sessler, J. Phys. D: Appl. Phys. **38**, 649 (2005).
[53]X. Qiu, A. Mellinger, and R. Gerhard, "In-situ Acoustical Investigation of the Polarization Build-up in Cellular Polypropylene Ferroelectrets," IEEE Trans. Dielectr. Electr. Insul. (to be published).
[54]M. Paajanen, M. Wegener, and R. Gerhard-Multhaupt, J. Phys. D: Appl. Phys. **34**, 2482 (2001).
[55]X. Qiu, A. Mellinger, and R. Gerhard, Appl. Phys. Lett. **92**, 052901 (2008).
[56]J. Hillenbrand and G. M. Sessler, *Annual Report Conference on Electrical Insulation and Dielectric Phenomena*, Victoria, Canada, 15–18 October 2000 (IEEE Service Center, Piscataway, NJ, 2000), pp. 161–165.
[57]I. Graz, A. Ebner, S. Bauer, C. Romanin, and H. Gruber, Appl. Phys. A: Mater. Sci. Process. **92**, 547 (2008).
[58]X. Qiu and R. Gerhard, Appl. Phys. Lett. **93**, 152902 (2008).
[59]M. Paajanen, H. Välimäki, and J. Lekkala, *Proceedings of the Tenth International Symposium on Electrets*, Delphi, Greece, 22–24 September 1999 (IEEE Service Center, Piscataway, NJ, 1999), pp. 735–738.
[60]G. M. Sessler and J. Hillenbrand, Appl. Phys. Lett. **75**, 3405 (1999).
[61]M. Paajanen, J. Lekkala, and H. Välimäki, IEEE Trans. Dielectr. Electr. Insul. **8**, 629 (2001).
[62]J. Hillenbrand, and G. M. Sessler, IEEE Trans. Dielectr. Electr. Insul. **7**, 537 (2000).
[63]G. S. Neugschwandtner, R. Schwödiauer, S. Bauer-Gogonea, S. Bauer, M. Paajanen, and J. Lekkala, J. Appl. Phys. **89**, 4503 (2001).
[64]J. A. Giacometti, S. Fedosov, and M. M. Costa, Braz. J. Phys. **29**, 269 (1999).
[65]M. Wegener, M. Paajanen, W. Wirges, and R. Gerhard-Multhaupt, *Proceedings of the 11th International Symposium on Electrets*, Melbourne, Australia, 1–3 October 2002 (IEEE Service Center, Piscataway, NJ, 2002), pp. 54–57.
[66]P. Fang, X. Qiu, W. Wirges, R. Gerhard, and L. Zirkel, "Polyethylene-naphthalate (PEN) Ferroelectrets: Cellular Structure, Piezoelectricity and Thermal Stability," IEEE Trans. Dielectr. Electr. Insul. (to be published).
[67]J. Kim, J. J. Ju, and M. Kim, Jpn. J. Appl. Phys., Part 1 **42**, 7304 (2003).
[68]M. Jäger, G. I. Stegeman, W. Brinker, S. Yılmaz, S. Bauer, W. H. G. Horsthuis, and G. R. Möhlmann, Appl. Phys. Lett. **68**, 1183 (1996).
[69]V. Taggi, F. Michelotti, M. Bertolotti, G. Petrocco, V. Foglietti, A. Donval, E. Toussaere, and J. Zyss, Appl. Phys. Lett. **72**, 2794 (1998).
[70]J. J. Ju, J. Kim, J. Y. Do, M. Kim, S. K. Park, S. Park, and M. Lee, Opt. Lett. **29**, 89 (2004).
[71]J. J. Ju, S. K. Park, S. Park, J. Kim, M. Kim, M. Lee, and J. Y. Do, Appl. Phys. Lett. **88**, 241106 (2006).
[72]R. F. Suárez, A. Mellinger, M. Wegener, W. Wirges, and R. Gerhard-Multhaupt, IEEE Trans. Dielectr. Electr. Insul. **13**, 1030 (2006).
[73]A. Mellinger, R. Flores Suárez, R. Singh, M. Wegener, W. Wirges, R. Gerhard, and S. B. Lang, Int. J. Thermophys. **29**, 2046 (2008).
[74]C.-D. Pham, A. Petre, L. Berquez, R. Flores Suárez, A. Mellinger, W. Wirges, and R. Gerhard, IEEE Trans. Dielectr. Electr. Insul. **16**, 676 (2009).
[75]R. F. Suárez, X. Qiu, L. Holländer, R. A. P. Altafim, W. Wirges, R. Gerhard, W. Jenninger, and J. Wagner, *Annual Report Conference on Electrical Insulation and Dielectric Phenomena*, Virginia Beach, USA, 18–20 October 2009 (IEEE Service Center, Piscataway, NJ, 2009).
[76]H. O. Jacobs and G. M. Whitesides, Science **291**, 1763 (2001).
[77]D. B. Wolfe, J. C. Love, B. D. Gates, G. M. Whitesides, R. S. Conroy, and M. Prentiss, Appl. Phys. Lett. **84**, 1623 (2004).
[78]B. Gross, R. Gerhard-Multhaupt, A. Berraissoul, and G. M. Sessler, J. Appl. Phys. **62**, 1429 (1987).
[79]R. V. Rao, P. M. Rao, and M. H. Shridhar, Nucl. Instrum. Methods Phys. Res. B **187**, 331 (2002).
[80]H. Nakayama, O. Sugihara, and N. Okamoto, Opt. Lett. **22**, 1541 (1997).
[81]O. Sugihara, Y. Che, N. Okamoto, H. Fujimura, C. Egami, and S. Umegaki, Appl. Phys. Lett. **73**, 3028 (1998).
[82]H. Nakayama, O. Sugihara, and N. Okamoto, Appl. Phys. Lett. **71**, 1924 (1997).
[83]H. Nakayama, H. Fujimura, C. Egami, O. Sugihara, R. Matsushima, and N. Okamoto, Appl. Opt. **37**, 1213 (1998).
[84]W. H. Wong, J. Zhou, and E. Y. B. Pun, Appl. Phys. Lett. **78**, 2110 (2001).
[85]H. Sun, A. Chen, B. C. Olbricht, J. A. Davies, P. A. Sullivan, Y. Liao, and L. Dalton, Opt. Express **16**, 6592 (2008).
[86]H. Kobayashi, M. Kubo, T. Tsukada, and M. Hozawa, Int. J. Heat Mass Transfer **45**, 865 (2002).
[87]M. Wegener, J. Hesse, T. Wegener, and R. Gerhard-Multhaupt, J. Appl. Phys. **91**, 3193 (2002).
[88]B. Dickens, E. Balizer, A. S. DeReggi, and S. C. Roth, J. Appl. Phys. **72**, 4258 (1992).
[89]E. Toussaere and P. Labbé, Opt. Mater. (Amsterdam, Neth.) **12**, 357 (1999).
[90]J. H. Jung, T. Kato, and T. Kinoshita, J. Appl. Phys. **90**, 801 (2001).
[91]G. Martin, S. Ducci, R. Hierle, D. Josse, and J. Zyss, Appl. Phys. Lett. **83**, 1086 (2003).
[92]J. H. Lin, N. D. Lai, C. H. Chiu, D. Y. Lin, G. W. Rieger, J. F. Young, F. S. Chien, and C. C. Hsu, Opt. Express **16**, 7832 (2008).
[93]F. S. Chien, C. Y. Lin, and C. C. Hsu, J. Phys. D: Appl. Phys. **41**, 235502 (2008).
[94]Y. Atassi, J. Chauvin, J. A. Delaire, J. F. Delouis, I. Fanton-Maltey, and K. Nakatani, Pure Appl. Chem. **70**, 2157 (1998).
[95]J. M. Nunzi, C. Fiorini, A. C. Etilé, and F. Kajzar, Pure Appl. Opt. **7**, 141 (1998).
[96]X. Liu, G. Xu, J. Si, P. Ye, Z. Li, and Y. Shen, J. Appl. Phys. **88**, 3848 (2000).
[97]N. Tsutsumi and C. Odane, J. Opt. Soc. Am. B **20**, 1514 (2003).
[98]W. Chalupczak, C. Fiorini, F. Charra, J. M. Nunzi, and P. Raimond, Opt. Commun. **126**, 103 (1996).
[99]C. Fiorini, F. Charra, J. M. Nunzi, and P. Raimond, J. Opt. Soc. Am. B **14**, 1984 (1997).
[100]C. Fiorini, F. Charra, P. Raimond, A. Lorin, and J.-M. Nunzi, Opt. Lett. **22**, 1846 (1997).
[101]K. Kitaoka, J. Si, T. Mitsuyu, and K. Hirao, Appl. Phys. Lett. **75**, 157 (1999).
[102]V. M. Churikov, M. F. Hung, C. C. Hsu, C. W. Shiau, and T. Y. Luh, Chem. Phys. Lett. **332**, 19 (2000).
[103]J. Guo, J. Si, G. Qian, J. Qiu, M. Wang, and K. Hirao, Chem. Phys. Lett. **381**, 677 (2003).
[104]Y. Jia, G. Wang, B. Guo, W. Su, and Q. Zhang, J. Opt. A, Pure Appl. Opt. **6**, 833 (2004).
[105]X. L. Jiang, L. Li, J. Kumar, and S. K. Tripathy, Appl. Phys. Lett. **69**, 3629 (1996).
[106]X. Liu, G. Xu, J. Si, P. Ye, Z. Li, and Y. Shen, Appl. Phys. B: Lasers Opt. **71**, 539 (2000).
[107]J. Si, T. Mitsuyu, P. Ye, Y. Shen, and K. Hirao, Appl. Phys. Lett. **72**, 762 (1998).
[108]J. Si, K. Kitaoka, T. Mitsuyu, P. X. Ye, and K. Hirao, J. Appl. Phys. **85**, 8018 (1999).
[109]J. Si and K. Hirao, Appl. Phys. Lett. **91**, 091105 (2007).
[110]A. Apostoluk, J. M. Nunzi, V. Boucher, A. Essahlaoui, R. Seveno, H. W. Gundel, C. Monnereau, E. Blart, and F. Odobel, Opt. Commun. **260**, 708 (2006).
[111]Z. Sekkat, P. Prêtre, A. Knoesen, W. Volksen, V. Y. Lee, R. D. Miller, J. Wood, and W. Knoll, J. Opt. Soc. Am. B **15**, 401 (1998).
[112]G. Xu, J. Si, X. Liu, Q. Yang, P. Ye, Z. Li, and Y. Shen, J. Appl. Phys. **85**, 681 (1999).
[113]G. Xu, J. Si, X. Liu, Q. Yang, P. Ye, Z. Li, and Y. Shen, Opt. Commun. **153**, 95 (1998).
[114]G. Xu, X. Liu, J. Si, P. Ye, Z. Li, and Y. Shen, Appl. Phys. B: Lasers Opt. **68**, 693 (1999).
[115]B. Guo, W. Su, Y. J. Jia, Z. C. Li, Q. J. Zhang, and G. M. Wang, Phys. Status Solidi B **242**, 1081 (2005).
[116]J. H. Jung and T. Kinoshita, Jpn. J. Appl. Phys., Part 1 **41**, 1587 (2002).
[117]D. Rollik, S. Bauer, and R. Gerhard-Multhaupt, J. Appl. Phys. **85**, 3282 (1999).
[118]B. Ploss, W. Y. Ng, H. L. W. Chan, B. Ploss, and C. L. Choy, Compos. Sci. Technol. **61**, 957 (2001).
[119]B. Ploss, B. Ploss, F. G. Shin, H. L. W. Chan, and C. L. Choy, IEEE Trans. Dielectr. Electr. Insul. **7**, 517 (2000).
[120]B. Ploss, B. Ploss, F. G. Shin, H. L. W. Chan, and C. L. Choy, Appl. Phys. Lett. **76**, 2776 (2000).
[121]I. Graz, M. Krause, S. Bauer-Gogonea, S. Bauer, S. P. Lacour, B. Ploss, M. Zirkl, B. Stadlober, and S. Wagner, J. Appl. Phys. **106**, 034503 (2009).
[122]S. A. Wilson, R. P. J. Jourdain, Q. Zhang, R. A. Dorey, C. R. Bowen, M. Willander, Q. Ul Wahab, M. Willander, S. M. Al-hilli, O. Nur, E. Quandt, C. Johansson, E. Pagounis, M. Kohl, J. Matovic, B. Samel, W. van der Wijngaart, E. W. H. Jager, D. Carlsson, Z. Djinovic, M. Wegener, C.

Moldovan, R. Iosub, E. Abad, M. Wendlandt, C. Rusu, and K. Persson, Mater. Sci. Eng. R. **56**, 1 (2007).
[123] R. Hasegawa, Y. Tanabe, M. Kobayashi, H. Tadokoro, A. Sawaoka, and N. Kawai, J. Polym. Sci., Part A: Polym. Chem. **8**, 1073 (1970).
[124] J. Scheinbeim, B. Nakafuku, B. A. Newman, and K. D. Pae, J. Appl. Phys. **50**, 4399 (1979).
[125] T. Hattori, M. Kanaoka, and H. Ohigashi, J. Appl. Phys. **79**, 2016 (1996).
[126] S. J. Kang, Y. J. Park, J. Hwang, H. J. Jeong, J. S. Lee, K. J. Kim, H. Kim, J. Huh, and C. Par, Adv. Mater. (Weinheim, Ger.) **19**, 581 (2007).
[127] L. Zhang, S. Ducharme, and J. Li, Appl. Phys. Lett. **91**, 172906 (2007).
[128] M. Nakanishi, H. Yamaji, O. Sugihara, H. Fujimura, C. Egami, and N. Okamoto, Mol. Cryst. Liq. Cryst. **349**, 15 (2000).
[129] E. Kim, Y. Xia, and G. M. Whitesides, Nature (London) **376**, 581 (1995).
[130] X. Zhao, A. Stoddart, S. P. Smith, E. Kim, Y. Xia, M. Prentiss, and G. M. Whitesides, Adv. Mater. (Weinheim, Ger.) **8**, 420 (1996).
[131] Y. Xia, E. Kim, and G. M. Whitesides, Chem. Mater. **8**, 1558 (1996).
[132] Y. J. Park, Y. S. Kang, and C. Park, Eur. Polym. J. **41**, 1002 (2005).
[133] S. S. Chebotaryov, E. M. Baitinger, A. A. Volegov, I. G. Margamov, I. V. Gribov, N. A. Moskvina, V. L. Kuznetsov, S. E. Evsyukov, and L. A. Pesin, Radiat. Phys. Chem. **75**, 2024 (2006).
[134] M. D. Duca, C. L. Plosceanu, and T. Pop, J. Appl. Polym. Sci. **67**, 2125 (1998).
[135] E. Katan, M. Narkis, and A. Siegmann, J. Appl. Polym. Sci. **70**, 1471 (1998).
[136] Y. Izumi, S. Kawanishi, S. Hara, D. Yoshikawa, and T. Yamamoto, Bull. Chem. Soc. Jpn. **71**, 2721 (1998).
[137] S. R. George, J. A. Leraas, S. C. Langford, and J. T. Dickinson, Appl. Surf. Sci. **255**, 9558 (2009).
[138] L. Torrisi and R. Percolla, Nucl. Instrum. Methods Phys. Res. B **117**, 387 (1996).
[139] S. Han, W. K. Choi, K. H. Yoon, and S. K. Koh, J. Appl. Polym. Sci. **72**, 41 (1999).
[140] S. Okuji, H. Boldyryeva, Y. Takeda, and N. Kishimoto, Nucl. Instrum. Methods Phys. Res. B **267**, 1557 (2009).
[141] H. M. Manohara, E. Morikawa, J. Choi, and P. T. Sprunger, J. Microelectromech. Syst. **8**, 417 (1999).
[142] E. Morikawa, J. Choi, H. M. Manohara, H. Ishii, K. Seki, K. K. Okudaira, and N. Ueno, J. Appl. Phys. **87**, 4010 (2000).
[143] J. Choi, H. M. Manohara, E. Morikawa, P. T. Sprunger, P. A. Dowben, and S. P. Palto, Appl. Phys. Lett. **76**, 381 (2000).
[144] G. L. J. A. Rikken, C. J. E. Seppen, S. Nijhuis, and E. W. Meijer, Appl. Phys. Lett. **58**, 435 (1991).
[145] O. Watanabe, M. Tsuchimori, and A. Okada, J. Mater. Chem. **6**, 1487 (1996).
[146] M. Nakanishi, O. Sugihara, N. Okamoto, and K. Hirota, Appl. Opt. **37**, 1068 (1998).
[147] O. Sugihara, M. Nakanishi, Y. Che, C. Egami, Y. Kawata, and N. Okamoto, Appl. Opt. **39**, 5632 (2000).
[148] F. Gillot, L. Mager, K. D. Dorkenoo, S. Méry, C. Carrré, and A. Fort, Chem. Phys. Lett. **379**, 203 (2003).
[149] J. P. Bombenger, L. Mager, D. Gindre, J. P. Vola, K. D. Dorkenoo, A. Fort, and C. Carré, Opt. Commun. **280**, 192 (2007).
[150] M. Saphiannikova and D. Neher, J. Phys. Chem. B **109**, 19428 (2005).
[151] C. J. Barrett, J. Mamiya, K. G. Yager, and T. Ikeda, Soft Matter **3**, 1249 (2007).
[152] V. Toshchevikov, M. Saphiannikova, and G. Heinrich, J. Phys. Chem. B **113**, 5032 (2009).
[153] T. Lippert and J. T. Dickinson, Chem. Rev. **103**, 453 (2003).
[154] C. Egami, Y. Kawata, Y. Aoshima, H. Takeyama, F. Iwata, O. Sugihara, M. Tsuchimori, O. Watanabe, H. Fujimura, and N. Okamoto, Opt. Commun. **157**, 150 (1998).
[155] Y. Che, O. Sugihara, C. Egami, H. Fujimura, Y. Kawata, N. Okamoto, M. Tsuchimori, and O. Watanabe, Jpn. J. Appl. Phys., Part 1 **38**, 6316 (1999).
[156] Y. Che, O. Sugihara, H. Fujimura, N. Okamoto, C. Egami, Y. Kawata, M. Tsuchimori, and O. Watanabe, Opt. Mater. (Amsterdam, Neth.) **21**, 79 (2003).
[157] G. Chen, Z. Xia, Y. Zhang, and H. Zhang, IEEE Trans. Dielectr. Electr. Insul. **6**, 831 (1999).
[158] Q. Zhang, P. A. Lewin, and P. E. Bloomfield, IEEE Trans. Ultrason. Ferroelectr. Freq. Control **44**, 1148 (1997) and references therein.
[159] M. Nakazawa, M. Tabaru, K. Nakamura, S. Ueha, and A. Maezawa, Jpn. J. Appl. Phys., Part 1 **46**, 4466 (2007).
[160] K. Sakaguchi, T. Sato, K. Koyama, S. Ikeda, S. Yamamizu, and Y. Wada, Jpn. J. Appl. Phys. **25**, 91 (1986) Suppl. 25-1.
[161] P. E. Bloomfield, IEEE Trans. Ultrason. Ferroelectr. Freq. Control **49**, 1300 (2002).
[162] N. Snis, E. Edqvist, U. Simu, and S. Johansson, Sens. Actuators A **144**, 314 (2008).
[163] E. Edqvist, N. Snis, and S. Johansson, J. Micromech. Microeng. **18**, 015007 (2008).
[164] E. Edqvist and E. Hedlund, J. Micromech. Microeng. **19**, 115019 (2009).
[165] R. Kacprzyk and E. Motyl, *Proceedings of the 8th International Symposium on Electrets*, Paris, France, 7–9 September 1994 (IEEE Service Center, Piscataway, NJ, 1994), pp. 703–708.
[166] R. Kacprzyk, E. Motyl, J. B. Gajewski, and A. Pasternak, J. Electrost. **35**, 161 (1995).
[167] R. Kacprzyk, A. Dobrucki, and J. B. Gajewski, J. Electros. **39**, 33 (1997).
[168] Z. Xia, R. Gerhard-Multhaupt, W. Künstler, A. Wedel, and R. Danz, J. Phys. D: Appl. Phys. **32**, L83 (1999).
[169] R. Gerhard-Multhaupt, W. Künstler, T. Görne, A. Pucher, T. Weinhold, M. Seiß, and Z. Xia, IEEE Trans. Dielectr. Electr. Insul. **7**, 480 (2000).
[170] M. Wegener, W. Wirges, K. Richter, W. Künstler, and R. Gerhard-Multhaupt, Proceedings of the fourth International Conference on Electric Charges in Non-Conductive Materials, Societé Française du Vide, Paris, France, 1-6 July 2001, pp. 257–260.
[171] M. Wegener, W. Wirges, W. Künstler, R. Gerhard-Multhaupt, B. Elling, M. Pinnow, and R. Danz, *Annual Report Conference on Electrical Insulation and Dielectric Phenomena*, Kitchener, Canada, 14–17 October 2001 (IEEE Service Center, Piscataway, NJ, 2001), pp. 100–103.
[172] Z. Hu and H. von Seggern, J. Appl. Phys. **98**, 014108 (2005).
[173] Z. Hu and H. von Seggern, J. Appl. Phys. **99**, 024102 (2006).
[174] R. A. C. Altafim, C. Dias, L. Gonçalves Neto, H. C. Basso, C. Murakami, P. R. Veronese, and E. F. Rodrigues, *Annual Report Conference on Electrical Insulation and Dielectric Phenomena*, New Mexico, USA, 19–22 October 2003 (IEEE Service Center, Piscataway, NJ, 2003), pp. 225–228.
[175] R. A. C. Altafim, H. C. Basso, L. Gonçalves Neto, L. Lima, R. A. P. Altafim, and C. V. de Aquino, *Annual Report Conference on Electrical Insulation and Dielectric Phenomena*, Tennessee, USA, 16–19 October 2005 (IEEE Service Center, Piscataway, NJ, 2005), pp. 669–672.
[176] R. A. C. Altafilm, H. C. Basso, R. A. P. Altafilm, L. Lima, C. V. de Aquino, L. Gonçalves Neto, and R. Gerhard-Multhaupt, IEEE Trans. Dielectr. Electr. Insul. **13**, 979 (2006).
[177] X. Zhang, J. Hillenbrand, and G. M. Sessler, Appl. Phys. A: Mater. Sci. Process. **84**, 139 (2006).
[178] R. A. P. Altafim, X. Qiu, W. Wirges, R. Gerhard, R. A. C. Altafim, H. C. Basso, W. Jenninger, and J. Wagner, J. Appl. Phys. **106**, 014106 (2009).
[179] E. M. Bazelyan and Y. P. Raizer, *Spark Discharge* (CRC, Boca Raton, FL, 1998).
[180] N. Yamauchi, Jpn. J. Appl. Phys., Part 1 **25**, 590 (1986).
[181] G. Xu, Q. G. Yang, J. H. Si, X. C. Liu, P. X. Ye, Z. Li, and Y. Q. Shen, Opt. Commun. **159**, 88 (1999).
[182] S. H. Lim, A. C. Rastogi, and S. B. Desu, J. Appl. Phys. **96**, 5673 (2004).
[183] R. C. G. Naber, C. Tanase, P. W. M. Blom, G. H. Gelinck, A. W. Marsman, F. J. Touwslager, S. Segayesh, and D. M. de Leeuw, Nature Mater. **4**, 243 (2005).
[184] K. N. N. Unni, S. Dabos-Seignon, and J. M. Nunzi, J. Phys. D: Appl. Phys. **38**, 1148 (2005).
[185] D. Gindre, A. Boeglin, A. Fort, L. Mager, and K. D. Dorkenoo, Opt. Express **14**, 9896 (2006).
[186] Q. Ling, D. Liaw, C. Zhu, D. S. Chan, E. Kang, and K. Neoh, Prog. Polym. Sci. **33**, 917 (2008).
[187] M. Mortezaie and G. Wade, in *Acoustic Imaging*, edited by M. Kaveh, R. K. Mueller, and J. F. Greenleaf (Plenum, New York, 1984), Vol. 13, pp. 345–354.
[188] M. Z. Sleva, W. D. Hunt, and R. D. Briggs, J. Acoust. Soc. Am. **96**, 1627 (1994).
[189] H. Hoislbauer, R. Schwödiauer, S. Bauer-Gogonea, and S. Bauer, *Proceedings of the 11th International Symposium on Electrets*, Melbourne, Australia, 1–3 October 2002 (IEEE Service Center, Piscataway, NJ, 2002), pp. 58–61.
[190] M. K. Hämäläinen, J. K. Parviainen, and T. Jaaskelainen, Rev. Sci. Instrum. **67**, 1598 (1996).
[191] J. Hillenbrand and G. M. Sessler, J. Acoust. Soc. Am. **116**, 3267 (2004).
[192] C. Y. Li, P. M. Wu, S. Lee, A. Gorton, M. J. Schulz, and C. H. Ahn, J. Microelectromech. Syst. **17**, 334 (2008).